On the Degree of Ill-Posedness of Multi-Dimensional Magnetic Particle Imaging

Tobias Kluth* Bangti Jin† Guanglian Li‡

June 22, 2018

Abstract

Magnetic particle imaging is an imaging modality of relatively recent origin, and it exploits the nonlinear magnetization response for reconstructing the concentration of nanoparticles. Since first invented in 2005, it has received much interest in the literature. In this work, we study one prototypical mathematical model in multi-dimension, i.e., the equilibrium model, which formulates the problem as a linear Fredholm integral equation of the first kind. We analyze the degree of ill-posedness of the associated linear integral operator by means of the singular value decay estimate for Sobolev smooth bivariate functions, and discuss the influence of various experimental parameters on the decay rate. In particular, applied magnetic fields with a field free point and a field free line are distinguished. The study is complemented with extensive numerical experiments.

Keywords: magnetic particle imaging; degree of ill-posedness; equilibrium model; singular value decay; Sobolev smooth bivariate functions.

1 Introduction

Magnetic particle imaging (MPI) is a relatively new imaging modality [11]. The main goal is to reconstruct a spatially dependent concentration of iron oxide nanoparticles by exploiting their superparamagnetic behavior. Measurements are obtained from multiple receive coils where a voltage is induced by particles' nonlinear response to the applied dynamic magnetic field using either field free point (FFP) [11] or field free line (FFL) [44] trajectories. These measurements can yield reconstructions with a high spatial/temporal resolution. Since the modality is free from harmful radiation, it is especially beneficial for in-vivo applications.

So far, MPI has been used for preclinical medical applications, and holds a significant potential for clinical applications. One application, already suggested at the beginning of the MPI development, is vascular imaging [11]. In in-vivo experiments, the potential for imaging blood flow was demonstrated using healthy mice [45]. Recently, it was studied for long-term circulating tracers [20]. The high temporal resolution allows tracking medical instruments [15], e.g., in angioplasty [38]. Other potential applications include cancer detection [47] and cancer treatment by hyperthermia [35].

In practice, MPI is usually modeled by a linear Fredholm integral equation of the first kind. This is motivated by the suppression of particle interactions due to nonmagnetic coating, which allows postulating a linear relationship between particle concentration and the measured voltage. However, precisely modeling MPI respectively formulating a physically accurate integral kernel for image reconstruction is still an unsolved problem due to various modeling errors in the particle dynamics and data acquisition, e.g., magnetization dynamics, particle-particle interactions and transfer function for analog filter; we refer interested readers to the survey paper [21] for further details. In the literature, the equilibrium model based on the Langevin

*Center for Industrial Mathematics, University of Bremen, Bibliothekstr. 5, 28357 Bremen, Germany (tkluth@math.uni-bremen.de)

†Department of Computer Science, University College London, Gower Street, London WC1E 6BT, UK (b.jin@ucl.ac.uk, bangti.jin@gmail.com)

‡Department of Mathematics, Imperial College London, London SW7 2AZ, UK. The work was partially carried out when the author was affiliated with Institut für Numerische Simulation and Hausdorff Center for Mathematics, Universität Bonn, Wegelerstraße 6, D-53115 Bonn, Germany. (lotusli0707@gmail.com, guanglian.li@imperial.ac.uk).

function has been used extensively to predict the signal behavior in MPI [24, 26]; see Section 2 below for details on the model, its derivation and the underlying assumptions.

The mathematical study on the MPI model is fairly scarce. The only work on FFP trajectories that we are aware of is the work [32]. In a 1D setup with FFP trajectories moving along a line for the equilibrium model, the authors [32] showed that in the limit of large particle diameters, the integral kernel is a Dirac-delta function, and thus the imaging problem is well-posed. Further, they analyzed a related problem which is independent of the FFP trajectory used, under the assumption that each spatial point is scanned multiple times with nonparallel trajectories. The problem was shown to be severely ill-posed in general, and in the large particle diameter limit, the smoothing property of the forward operator improves with the spatial dimension d. Also, if a FFL is moved by a drive field in its perpendicular direction, the problem can be formulated using Radon transform, followed by a convolution with a kernel involving the mean magnetic moment [25]. However, the theoretical analysis of general FFL trajectories remains missing.

In this work, we present a study on the degree of ill-posedness of the MPI inverse problem. Historically, the idea of distinguishing mildly, moderately and severely ill-posed problems can be traced at least back to Grace Wahba [42]. Since the 1980s, the concept "degree of ill-posedness" for linear inverse problems has been popular. Roughly, it refers to the decay behavior of the singular values (SVs) σ_n: $\sim n^{-\nu}$ with small $0 < \nu < 1$ for mildly ill-posed problems, with $1 \leq \nu < \infty$ for moderately ill-posed ones, and otherwise for severely ill-posed ones, e.g., $e^{-\nu n}$ with $\nu > 0$. There are at least two reasons to look at the SV decay rate (see, e.g., [7, 17]). First, it characterizes the degree of ill-posedness of the imaging problem, which is one factor in determining the resolution limit of the image reconstruction step, when the data accuracy and model accuracy etc. are given. Second, the analysis also sheds insight into how to improve the resolution by properly changing the experimental setting. Hence, over the past few decades, SV decay estimates have received much interest for a number of inverse problems, especially in the context of computed tomography.

In this work, we study the degree of ill-posedness of MPI via SV decay of the associated linear integral operator. Our analysis relies crucially on the SV decay estimate for Sobolev smooth bivariate functions [14], and its extension to less regular bivariate functions. The extension seems still unavailable and will be given in this work, and the result is of independent interest. Our results give upper bounds on SV decay rates, which indicate the (best possible) degree of ill-posedness of the MPI model. We discuss the following three cases separately: nonfiltered model, limit model and filtered model, in order to illuminate the influences of experimental parameters, e.g., particle size and the regularity of the analog filter. Further, we conduct extensive numerical experiments to complement the analysis. When completing the paper, the authors became aware of the work [9], where Erb et al. showed the exponential ill-posedness of a 1D MPI model. It differs substantially from this work in the main focus (multi-dimensional model) and analytical tools.

Note that the SV decay is only one factor for the "level of recovery chances" to linear ill-posed problems, as already emphasized by Louis [30] in 1989, with the other being "solution smoothness with respect to the character of the forward operator". Only both factors and their interplay allow realistic error estimates on the reconstructions from noisy data, and the degree of ill-posedness must be put into the context of regularization. Such an analysis is beyond the scope of this work; see the works [33, 16] for relevant results.

The remainder of the paper is organized as follows. In Section 2, we describe the equilibrium model, and in Section 3, the SV decay estimate for Sobolev smooth bivariate functions. Then in Section 4, we analyze the decay rate for the integral operators for nonfiltered and filtered models, and discuss the influence of various factors, e.g., spatial dimensionality d and particle parameter β. In Section 5, we present numerical results to support the analytical findings, and finally, in Section 6, we give concluding remarks. Throughout, we denote by C with/without subscript a generic constant which may differ at each occurrence.

2 The equilibrium model

Now we describe the equilibrium model, one prototypical mathematical model for MPI.

2.1 Preliminaries

MPI is inherently a 3D problem, and thus vector valued functions remain 3D even if the domain Ω of the spatial variable x is a subset of a d-dimensional affine subspace $E_d \subset \mathbb{R}^3$. Let $\Omega \subset E_d$, $d = 1, 2, 3$, be a

bounded domain with a (strong) Lipschitz boundary $\partial\Omega$ in E_d. Further, let $T > 0$ denote the maximal data acquisition time and $I := (0, T)$ the time interval during which the measurement process takes place. The temporal derivative of any function $g : I \to \mathbb{R}^d$ is denoted by $\dot{g}$.

In MPI, the measured signal $v_\ell : I \to \mathbb{R}$, $\ell = 1, \dots, L$, obtained at $L \in \mathbb{N}$ receive coils, is given by

$$v_\ell(t) = \int_I \int_\Omega c(x) a_\ell(t - t') \kappa_\ell(x, t) \mathrm{d}x\mathrm{d}t' + \underbrace{\int_I \int_{\mathbb{R}^3} a_\ell(t - t') \mu_0 p_\ell(x)^t \dot{H}(x, t) \mathrm{d}x\mathrm{d}t'}_{=v_{\mathrm{E},\ell}(t)}, \tag{2.1}$$

where the superscript t denotes the transpose of a vector, $c : \Omega \to \mathbb{R}^+ \cup \{0\}$ is the concentration of the magnetic nanoparticles and $\kappa_\ell : \Omega \times I \to \mathbb{R}$, $\ell = 1, \dots, L$, represent the system functions characterizing the magnetization behavior of nanoparticles. The positive constant μ_0 is magnetic permeability in vacuum. The scalar functions $a_\ell : \bar{I} := [-T : T] \to \mathbb{R}$, $\ell = 1, \dots, L$, are the analog filter in the signal acquisition chain, and in practice, they are often band stop filters adapted to excitation frequencies of the drive field so as to minimize the adverse influence of the excitation signal $v_{\mathrm{E},\ell}$ during digitization. The functions $p_\ell : \mathbb{R}^3 \to \mathbb{R}^3$, $\ell = 1, \dots, L$, denote the vector field which characterizes the sensitivity profile of the receive coils and can be spatially dependent. Throughout, it is assumed that the applied magnetic field $H : \mathbb{R}^3 \times I \to \mathbb{R}^3$ and the filters $\{a_\ell\}_{\ell=1}^L$ are chosen in a way such that all excitation signals $v_{\mathrm{E},\ell} = 0$, $\ell = 1, \dots, L$.

Remark 2.1. *The assumption on the excitation signals $\{v_{\mathrm{E},\ell}\}_{\ell=1}^L$ is commonly made, which, however, may be not fulfilled in MPI applications [40, 22]. Note that in the model (2.1), we have absorbed the minus sign into the measurement to make the notation more consistent with literature on integral equations.*

The applied magnetic field $H(x, t)$ can be characterized by a spatially dependent magnetic field $g : \mathbb{R}^3 \to \mathbb{R}^3$ and a time-dependent homogeneous magnetic field $h : I \to \mathbb{R}^3$, and the field $H(x, t)$ is given by their superposition, i.e., $H(x, t) = g(x) - h(t)$. The field g, named *selection field*, ensures that a field-free-region is generated. Generally, g is assumed to be linear such that it can be represented by a constant matrix $G \in \mathbb{R}^{3\times3}$. The field h, named *drive field*, then moves the field-free-region along a certain trajectory. Two MPI methodologies are distinguished by the field free region, whether a FFP is generated ($\mathrm{rank}(G) = 3$) or a FFL is used ($\mathrm{rank}(G) = 2$). For the FFL approach, it was also proposed to rotate the selection field g over time such that the FFL is rotated [44], and then the selection field is given by $g : \mathbb{R}^3 \times I \to \mathbb{R}^3$ with $g(x, t) = P(t)^t G P(t) x$ where $P(t) : I \to \mathbb{R}^{3\times3}$ is a rotation matrix for all $t \in I$.

The functions $\{\kappa_\ell\}_{\ell=1}^L$ can be expressed using the receive coil sensitivities $\{p_\ell\}_{\ell=1}^L$ and the particles' mean magnetic moment vector $\bar{m} : \Omega \times I \to \mathbb{R}^3$ as $\kappa_\ell = \mu_0 p_\ell^t \dot{\bar{m}}$. This relation follows from Faraday's law and the law of reciprocity [24]. Then the inverse problem is to find the concentration $c : \Omega \to \mathbb{R}^+ \cup \{0\}$ from $\{v_\ell\}_{\ell=1}^L$:

$$v_\ell(t) = \int_I \int_\Omega c(x) a_\ell(t - t') \kappa_\ell(x, t') \mathrm{d}x\mathrm{d}t', \quad \text{with } \kappa_\ell = \mu_0 p_\ell^t \dot{\bar{m}}. \tag{2.2}$$

In the model (2.2), the linear dependence on the concentration c is derived under the assumption that particle-particle interactions can be neglected. However, there is experimental evidence that these interactions can affect the particle signal [31].

2.2 Equilibrium MPI model

To specify the MPI model, it remains to describe the mean magnetic moment vector $\bar{m}(x, t)$ of nanoparticles. There are several possible models, e.g., Fokker-Planck equation or stochastic Landau-Lifschitz-Gilbert equation [21]. The most extensively studied model in MPI is based on the assumptions that the applied magnetic field $H(x, t)$ is static, the particles are in equilibrium, and $\bar{m}(x, t)$ immediately follows the magnetic field $H(x, t)$. Then by Langevin theory for paramagnetism, $\bar{m}(x, t)$ is given by

$$\bar{m}(x, t) = m_0 \mathcal{L}_\beta(|H(x, t)|) \frac{H(x, t)}{|H(x, t)|},$$

where the parameter m_0 is particle's magnetic moment, $|\cdot|$ denotes the Euclidean norm of vectors, and $\mathcal{L}_\beta : \mathbb{R} \to \mathbb{R}$ is the (scaled) Langevin function given by

$$\mathcal{L}_\beta(z) = \coth(\beta z) - (\beta z)^{-1}, \tag{2.3}$$

where β is a given positive parameter. The Langevin function $\mathcal{L}_\beta(z)$ captures the nonlinear response to the applied magnetic field. The resulting model is termed as *equilibrium model* below.

Remark 2.2. *Physically, the parameters m_0 and β are determined by the saturation magnetization $M_{\rm S}$ of the core material, the volume $V_{\rm C}$ of the single-domain particle's core, the temperature $T_{\rm B}$, and Boltzmann constant $k_{\rm B}$, i.e., $m_0 = M_{\rm S}V_{\rm C}$ and $\beta = \mu_0 m_0/(k_{\rm B}T_{\rm B})$. Note that β also depends on the particle diameter D through m_0. At room temperature 293 K, particles consisting of magnetite with a typical diameter D of 30 nm (20 nm) are characterized by $\beta \approx 2.1 \times 10^{-3}$ (0.6×10^{-3}).*

The function $L_\beta(z)$ is a smooth approximation to the sign function: for any fixed $0 < \beta < \infty$, it belongs to $C^\infty(\mathbb{R})$, and as $\beta \to \infty$, it recovers the sign function $\mathrm{sign}(z)$.

Lemma 2.1. *The Langevin function $L_\beta(z)$ has the following properties:* (i) *For any $z \in \mathbb{R}$, there holds $\lim_{\beta\to\infty} \mathcal{L}_\beta(z) = \mathrm{sign}(z)$; and* (ii) *The function $\frac{L_\beta(\sqrt{z})}{\sqrt{z}} \in C_B^\infty([0,\infty))$.*

Proof. First, recall the following expansions for the $\coth(z)$:

$$\coth(z) = \frac{1}{z} + \frac{z}{3} - \frac{z^3}{45} + \frac{2}{945}z^5 - \ldots + \frac{2^{2n}B_{2n}}{(2n)!}z^{2n-1} + \ldots \quad (|z| < \pi), \tag{2.4}$$

where B_n is the nth Bernoulli number [1, 4.5.67, p. 85]. Meanwhile, for any $z > 0$, we have

$$\coth(z) = \frac{e^z + e^{-z}}{e^z - e^{-z}} = 1 + \frac{2e^{-2z}}{1 - e^{-2z}} = 1 + 2\sum_{j=1}^{\infty} e^{-2jz}, \tag{2.5}$$

and a similar series expansion holds for $z < 0$. Now assertion (i) follows directly from (2.5). For part (ii), it suffices to show $\beta = 1$. For $0 \le z < \pi^2$, it follows from (2.4) and the definition of $L_1(z)$ that

$$\frac{L_1(\sqrt{z})}{\sqrt{z}} = \frac{1}{3} - \frac{z}{45} + \frac{2}{945}z^2 - \ldots + \frac{2^{2n}B_{2n}}{(2n)!}z^{n-1} + \ldots,$$

which is smooth in z (and convergent for any $0 \le z < \pi^2$). The assertion for $z > 1$ follows from (2.5). □

In summary, the inverse problem for the equilibrium model is to recover the concentration c from

$$\begin{cases} v_\ell(t) = \displaystyle\int_I \int_\Omega c(x) a_\ell(t - t') \kappa_\ell(x, t') \mathrm{d}x\mathrm{d}t', \\ \kappa_\ell(x,t) = \mu_0 m_0 p_\ell^t \dfrac{\mathrm{d}}{\mathrm{d}t}\left[\dfrac{\mathcal{L}_\beta(|H|)}{|H|} H\right], \end{cases} \tag{2.6}$$

for $\ell = 1, \ldots, L$ and the magnetic field $H : \Omega \times I \to \mathbb{R}^3$ is given by $H(x,t) = g(x) - h(t)$, where $g : \Omega \to \mathbb{R}^3$ and $h : I \to \mathbb{R}^3$. For MPI, a common choice is $g(x) = Gx$ and $h(t) = A(\sin(f_i t))_{i=1}^3$, where $A \in \mathbb{R}^{3\times 3}$ is a diagonal matrix with $1 \le \mathrm{rank}(A) \le d$, $f_i > 0$, and a constant matrix $G \in \mathbb{R}^{3\times 3}$ with $\mathrm{tr}(G) = 0$. Below, for the matrix G, we distinguish two cases: (i) G has full rank such that a FFP is generated, and (ii) $\mathrm{rank}(G) = 2$ such that a FFL is generated (only for 3D).

In the model (2.6), all vectors belong to $\mathbb{R}^3$, which reflects the intrinsic 3D nature of the MPI imaging problem. However, for a spatial domain $\Omega \subset \mathbb{R}^d$, $d = 1, 2$, the dimensionality of the vectors and matrices can be taken to be d, by properly restricting to subvectors/submatrices, which is feasible under the assumption that $G^{-1}h(t) \in \Omega$, for any $t \in I$ (i.e., field free region is contained in Ω). Specifically, the d-dimensional case, for $d = 1, 2$, can be constructed by assuming that the concentration c is a Dirac δ-distribution with respect to the orthogonal complement of the affine subspace $E_d \subset \mathbb{R}^3$, i.e., $c(x) = c_d(x_1)\delta(x_2)$, where $x = x_1 + x_2$ with $x_1 \in E_d$, $x_2 \in E_d^\perp$, and $c_d : \Omega \subset E_d \to \mathbb{R}^+ \cup \{0\}$. The parametrization of the domain $\Omega \subset E_d$ then allows reformulating the integral in (2.6) in terms of $\Omega_d \subset \mathbb{R}^d$. Given the affine linear parametrization $\Gamma : \Omega_d \to \Omega$, (2.6) can be stated with respect to $\tilde{c}_d : \Omega_d \to \mathbb{R}^+ \cup \{0\}$, $\tilde{c}_d(x) = c_d(\Gamma(x))$. This convention will be adopted in the analysis below, by directly writing $h(t) \in I \to \mathbb{R}^d$ etc.

3 Singular value decay for Sobolev smooth bivariate functions

Now we describe SV decay for Sobolev smooth bivariate functions, which is the main technical tool for studying degree of ill-posedness in Section 4.

3.1 Preliminaries on function spaces

First, we recall Sobolev spaces and Bochner-Sobolev spaces, which are used extensively below. For any index $\alpha \in \mathbb{N}^d$, $|\alpha|$ is the sum of all components. Given a domain $D \subset \mathbb{R}^d$ with a Lipschitz continuous boundary, for any $m \in \mathbb{N}$, $1 \le p \le \infty$, we follow [2] and define the Sobolev space $W^{m,p}(D)$ by

$$W^{m,p}(D) = \big\{u \in L^p(D) : D^\alpha u \in L^p(D) \text{ for } 0 \le |\alpha| \le m\big\}.$$

It is equipped with the norm

$$\|u\|_{W^{m,p}(D)} = \begin{cases} \Big(\sum\limits_{0\le|\alpha|\le m} \|D^\alpha u\|^p_{L^p(D)}\Big)^{\frac{1}{p}}, & \text{if } 1 \le p < \infty, \\ \max\limits_{0\le|\alpha|\le m} \|D^\alpha u\|_{L^\infty(D)}, & \text{if } p = \infty. \end{cases}$$

The space $W^{m,p}_0(D)$ is the closure of $C^\infty_0(D)$ in $W^{m,p}(D)$. Its dual space is denoted by $W^{-m,p'}(D)$, with $\frac{1}{p} + \frac{1}{p'} = 1$, i.e., p' is the conjugate exponent of p. Also we use $H^m(D) = W^{m,2}(D)$, and $H^m_0(D) = W^{m,2}_0(D)$. The fractional order Sobolev space $W^{s,p}(D)$, $s \ge 0, s \notin \mathbb{N}$, can be defined by interpolation [2]. It can be equivalently defined by a Sobolev–Slobodeckiĭ seminorm $|\cdot|_{W^{s,p}(D)}$. For $0 < s < 1$, it is defined by

$$|u|^p_{W^{s,p}(D)} := \int_D \int_D \frac{|u(x) - u(y)|^p}{|x - y|^{d+sp}} \,\mathrm{d}x\mathrm{d}y, \tag{3.1}$$

and the full norm $\|u\|_{W^{s,p}(D)} = (\|u\|^p_{L^p(D)} + |u|^p_{W^{s,p}(D)})^{\frac{1}{p}}$. For $s > 1$, it can be defined similarly.

We state a result on pointwise multiplication on Sobolev spaces [4, Theorem 7.5].

Theorem 3.1. *Let $D \subset \mathbb{R}^d$, $d = 1, 2, 3$. Assume that s_i, s $(i = 1, 2)$ are real numbers satisfying $s_i \ge s \ge 0$ and $s_1 + s_2 - s > \frac{d}{2}$. Then for some constant $C(s_1, s_2, s, d)$, there holds*

$$\|uv\|_{H^s(D)} \le C(s_1, s_2, s, d)\|u\|_{H^{s_1}(D)}\|v\|_{H^{s_2}(D)} \quad \forall u \in H^{s_1}(D), v \in H^{s_2}(D).$$

Suppose X is a Banach space, with the norm denoted by $\|\cdot\|_X$. Then, for any $p \in \mathbb{N}$, we denote by $H^p(I; X)$ the Bochner space of functions $v : I \to X$ such that $v(t)$ and its weak derivatives (in time) up to order p, i.e., $\dot v(t), \ldots, v^{(p)}(t)$, all exist and belong to $L^2(I; X)$. The norm on $H^p(I; X)$ is defined by

$$\|v\|^2_{H^p(I;X)} = \sum_{j=0}^{p} \int_I \|v^{(j)}(t)\|^2_X \mathrm{d}t.$$

Then for any $s \ge 0$, we can define $H^s(I; X)$ by means of interpolation, and equivalently using the Sobolev-Slobodeckiĭ seminorm [18]. For example, for $s \in (0, 1)$, then the seminorm $|\cdot|_{H^s(I;X)}$ is defined by

$$|v|^2_{H^s(I;X)} = \int_I \int_I \frac{\|v(t_1, \cdot) - v(t_2, \cdot)\|^2_X}{|t_1 - t_2|^{1+2s}} \mathrm{d}t_1\mathrm{d}t_2,$$

and $\|v\|_{H^s(I;X)} = (\|v\|^2_{L^2(I;X)} + |v|^2_{H^s(I;X)})^{\frac{1}{2}}$. We shall use the case $X = L^2(D)$ extensively. The space $H^s(0, T; L^2(D))$ is isomorphic to $H^s(0, T) \times L^2(D)$ and $L^2(D; H^s(0, T))$, i.e., $H^s(0, T; L^2(D)) \simeq H^s(0, T) \times L^2(D) \simeq L^2(D; H^s(0, T))$ (see, e.g., [18, Proposition 1.2.24, p. 25] for the isomorphism $L^2(I; L^2(D)) \simeq L^2(D; L^2(I))$, from which the general case may be derived). Then by [18, Proposition 1.3.3, p. 39], we have $L^2(D; H^{-s}(I)) \simeq H^{-s}(I; L^2(D))$. We shall use these isomorphisms frequently below.

Now we give two results on the composition operator on $H^s(I; L^\infty(D))$ and $H^s(D; W^{1,\infty}(I))$.

Lemma 3.1. *The following two statements hold.*

(i) *For $v \in H^s(I;L^\infty(D)) \cap L^\infty(I;L^\infty(D))$ $(s \geq 0)$ and $g \in C_B^k(\mathbb{R})$ $(k \geq [s]+1)$, $g \circ v \in H^s(I;L^\infty(D))$.*

(ii) *For $v \in H^s(D;W^{1,\infty}(I)) \cap L^\infty(D;W^{1,\infty}(I))$ $(s \geq 0)$ and $g \in C_B^k(\mathbb{R})$ $(k \geq [s]+2)$, $g \circ v \in H^s(D;W^{1,\infty}(I))$.*

Proof. By the definition (3.1) and the mean value theorem, for $0 < s < 1$, since $v \in L^\infty(I;L^\infty(D))$, we have

$$\begin{aligned}
|g \circ v|^2_{H^s(I;L^\infty(D))} &= \int_I \int_I \frac{\|g(v(t_1,\cdot)) - g(v(t_2,\cdot))\|^2_{L^\infty(D)}}{|t_1 - t_2|^{1+2s}} \mathrm{d}t_1 \mathrm{d}t_2 \\
&\leq \int_I \int_I \frac{\sup_{\xi\in\mathbb{R}} |g'(\xi)|^2 \|v(t_1,\cdot) - v(t_2,\cdot)\|^2_{L^\infty(D)}}{|t_1 - t_2|^{1+2s}} \mathrm{d}t_1 \mathrm{d}t_2 \\
&\leq \sup_{\xi\in\mathbb{R}} |g'(\xi)|^2 |v|^2_{H^s(I;L^\infty(D))} < \infty.
\end{aligned}$$

The case $s \geq 1$ follows similarly by the chain rule and Theorem 3.1. For example, for $1 < s < 2$, by chain rule, $\frac{\mathrm{d}}{\mathrm{d}t}(g \circ v)(t) = (g' \circ v)\dot{v}$. Since $\dot{v} \in H^{s-1}(I;L^\infty(\Omega))$ and $g' \circ v \in H^1(I;L^\infty(\Omega))$, Theorem 3.1 implies $\frac{\mathrm{d}}{\mathrm{d}t}(g \circ v) \in H^{s-1}(I;L^\infty(\Omega))$, showing the assertion for $s \in (1,2)$.

For any $v \in L^\infty(D;W^{1,\infty}(I))$, by the chain rule, mean value theorem and triangle inequality, direct computation gives that for any $x_1, x_2 \in D$

$$\begin{aligned}
\|g(v(\cdot,x_1)) - g(v(\cdot,x_2))\|_{W^{1,\infty}(I)} &= \|g(v(\cdot,x_1)) - g(v(\cdot,x_2))\|_{L^\infty(I)} \\
&\quad + \|g'(v(\cdot,x_1))\dot{v}(\cdot,x_1) - g'(v(\cdot,x_2))\dot{v}(\cdot,x_2)\|_{L^\infty(I)} \\
&\leq C\|(v(\cdot,x_1) - v(\cdot,x_2)\|_{W^{1,\infty}(I)} + C\|v(\cdot,x_1) - v(\cdot,x_2)\|_{L^\infty(I)} \|\dot{v}(\cdot,x_1)\|_{L^\infty(I)},
\end{aligned}$$

where the constant C depends only on $\|g\|_{C_B^2(\mathbb{R})}$. By the definition (3.1), for $0 < s < 1$, we have

$$\begin{aligned}
|g \circ v|^2_{H^s(D;W^{1,\infty}(I))} &= \int_D \int_D \frac{\|g(v(\cdot,x_1)) - g(v(\cdot,x_2))\|^2_{W^{1,\infty}(I)}}{|x_1 - x_2|^{d+2s}} \mathrm{d}x_1 \mathrm{d}x_2 \\
&\leq C \int_D \int_D \frac{\|v(\cdot,x_1) - v(\cdot,x_2)\|^2_{W^{1,\infty}(I)}}{|x_1 - x_2|^{d+2s}} \mathrm{d}x_1 \mathrm{d}x_2 \\
&\quad + C \int_D \int_D \frac{\|v(\cdot,x_1) - v(\cdot,x_2)\|^2_{L^\infty(I)} \|\dot{v}(\cdot,x_1)\|^2_{L^\infty(I)}}{|x_1 - x_2|^{d+2s}} \mathrm{d}x_1 \mathrm{d}x_2 \\
&\leq C(|v|^2_{H^s(D;W^{1,\infty}(I))} + |v|^2_{H^s(D;L^\infty(I))} \|v\|^2_{L^\infty(D;L^\infty(I))}) < \infty.
\end{aligned}$$

This shows the assertion for $0 < s < 1$. The case $s \geq 1$ follows similarly as part (i). □

3.2 Singular value decay

Now we describe our main tool of the analysis, i.e., SV decay estimates for Sobolev smooth bivariate functions. The study of eigenvalues of integral operators with a kernel function has a rather long history. The monographs [37] and [28] contain a wealth of relevant results. However, the results in these works are concerned with two variables defined on the same domain, which do not handle the integral kernel $\kappa(x,t)$ directly. We shall use the recent result due to Griebel and Li [14] (see [14, Theorem 3.2]), for the nonfiltered model in Section 4.1; see [37, Chapter 2] for an introduction to the Lorentz sequence space $\ell_{p,w}$.

Theorem 3.2. *Suppose that $D \subset \mathbb{R}^d$ satisfies the strong local Lipschitz condition. Let $\kappa(x,y) \in L^2(\Omega, H^s(D))$, $s \geq 0$. Then the SVs σ_n of the associated integral operator satisfy*

$$\sigma_n \leq \mathrm{diam}(D)^s C_{\mathrm{em}}(d,s)^{\frac{1}{2}} C_{\mathrm{ext}}(D,s)^{\frac{1}{2}} \|\kappa\|_{L^2(\Omega,H^s(D))} n^{-\frac{1}{2}-\frac{s}{d}},$$

where the constant $C_{\mathrm{ext}}(D,s)$ depends only on D and s (for Sobolev extension), $C_{\mathrm{em}}(d,s)$ is an embedding constant for $\ell_{\frac{d}{d+2s},1} \hookrightarrow \ell_{\frac{d}{d+2s},\infty}$, and $\mathrm{diam}(D)$ is the diameter of the domain D.

Note that the result in Theorem 3.2 requires $s \geq 0$, which does not cover less regular kernels for the limit model in Section 4.2 below. For general rough kernels, the spectral theory is largely open [37, 28]. Below we analyze the kernel $f : D \times I \to \mathbb{R}$ defined by (with $d > 1$ being the dimension of the domain D)

$$f(x,t) := |Gx - h(t)|^{-\frac{d}{2}}.$$

We will make the following assumption.

Assumption 3.1. *Suppose that the matrix $G \in \mathbb{R}^{d\times d}$ is invertible, and the trajectory $h(t) : I \to \mathbb{R}^d$ satisfies*

(i) *There exists C_h such that $C_h := \sup_{t\in[0,T]} |\dot{h}(t)|^{-1} < \infty$.*

(ii) *For any $t \in I$, $G^{-1}h(t) \in D$; and there exists at most N_h distinct $t \in I$ such that $h(t) = Gx$, for any $x \in D$.*

Remark 3.1. *The condition $G^{-1}h(t) \in D$ describes that the FFP moves within the physical domain D, and the domain D is properly covered by the trajectories. The analysis remains valid if the condition holds for any open subinterval of I. If for all $t \in I$, $G^{-1}h(t) \notin D$, then $|Gx - h(t)|^r$ belongs to $C^\infty(\overline{I}; L^2(D))$ for smooth trajectories $h(t)$, and the analysis in Section 4.1 applies directly.*

First, by the proof of Lemma 4.1 below, we have $f(x,t) \in L^2(I; L^p(D))$ for any $p \in (1,2)$. Now we define the associated integral operator $\mathcal{S} : L^{p'}(D) \to L^2(I)$ with $f(x,t)$ as its kernel, and its adjoint operator $\mathcal{S}^* : L^2(I) \to L^p(D)$, respectively, by

$$(\mathcal{S}v)(t) = \int_D f(x,t)v(x)\mathrm{d}x \quad \text{and} \quad (\mathcal{S}^*v)(x) = \int_I f(x,t)v(t)\mathrm{d}t.$$

Let $\mathcal{R} : L^{p'}(D) \to L^p(D)$ by $\mathcal{R} = \mathcal{S}^*\mathcal{S}$. By construction, $\mathcal{R}$ is an integral operator with its kernel $R \in L^p(D) \times L^p(D) : D \times D \to \mathbb{R}$ given by

$$R(x,x') = \int_I f(x,t)f(x',t)\mathrm{d}t. \tag{3.2}$$

Now we give mapping properties of $\mathcal{S}$. See [2, pp. 221–228] for an introduction to Lorentz spaces $L^{p,\infty}(D)$.

Lemma 3.2. *For $d = 2, 3$, let Assumption 3.1 be fulfilled. Then the following statements hold.*

(i) *For all $q > 2$, the operator $\mathcal{S} : L^q(D) \to L^\infty(I)$ is bounded;*

(ii) *For all $p \in (\frac{2(d-1)}{d}, 2)$ and $q = \frac{2p}{d(2-p)}$, the operator $\mathcal{S} : L^p(D) \to L^q(I)$ is bounded. In addition, $\mathcal{S}$ is compact from $L^2(D)$ to $L^2(I)$.*

Proof. By the proof of Lemma 4.1 below, $v(t) := \|f(\cdot,t)\|_{L^{2-\epsilon}(D)} \in L^\infty(I)$ for any $\epsilon > 0$. Together with [29, Theorem 6.1, p. 99], it implies that $\mathcal{S}$ is bounded from $L^q(D)$ to $L^\infty(I)$ for all $q > 2$.

The proof of assertion (ii) is inspired by the proof of Theorem 8.10 of [29, p. 165]. It relies on Stein-Weiss interpolation theorem (see, e.g., [29, Theorem 8.2, p. 150] and [39, Chapter 5]). First, we claim that there is $C > 0$ such that for any $p \in (\frac{2(d-1)}{d}, 2)$ and $q = \frac{2p}{(2-p)d}$, there holds

$$\|\mathcal{S}\chi_A\|_{L^{q,\infty}(I)} \leq C|A|^{\frac{1}{p}} \tag{3.3}$$

for all measurable subsets $A \subset D$ with finite measure, where χ_A is the characteristic function of A. If the estimate (3.3) holds, then by Stein-Weiss interpolation theorem, $\mathcal{S}$ is bounded from $L^p(D)$ to $L^q(I)$ for all $p \in (\frac{2(d-1)}{d}, 2)$ and $q = \frac{2p}{d(2-p)}$. Then Theorem 5.4 of [29, p. 83] implies that $\mathcal{S}$ is compact from $L^2(D)$ to $L^2(I)$. Hence, it suffices to prove the estimate (3.3).

First, by Hölder's inequality with an exponent $\gamma \in (\frac{1}{q}, \frac{1}{p})$, we obtain

$$\begin{aligned}\mathcal{S}\chi_A(t) &= \int_A |Gx - h(t)|^{-\frac{d}{2}}\mathrm{d}x = \int_A |Gx - h(t)|^{-(\frac{d}{2}-\frac{1}{q})}|Gx - h(t)|^{-\frac{1}{q}}\mathrm{d}x \\ &\leq \Big(\int_A |Gx - h(t)|^{-(\frac{d}{2}-\frac{1}{q})(1-\gamma)^{-1}}\mathrm{d}x\Big)^{1-\gamma}\Big(\int_A |Gx - h(t)|^{-\frac{1}{q\gamma}}\mathrm{d}x\Big)^{\gamma}.\end{aligned} \tag{3.4}$$

Let $s := (\frac{d}{2} - \frac{1}{q})(1-\gamma)^{-1}$, and let $B(G^{-1}h(t), \rho) := \{x \in \mathbb{R}^d : |x - G^{-1}h(t)| \le \rho\}$ be the ball centered at $G^{-1}h(t)$ with a radius ρ satisfying $|B(G^{-1}h(t), \rho)| = |A|$, which implies $|A| = |\mathbb{S}^{d-1}|\rho^d$, where $|\mathbb{S}^{d-1}|$ denotes the volume of the unit sphere in $\mathbb{R}^d$. Then by equation (8.33) of [29, p. 154], we have

$$\begin{aligned}
&\int_A |x - G^{-1}h(t)|^{-s}\mathrm{d}x - \int_{B(G^{-1}h(t),\rho)} |x - G^{-1}h(t)|^{-s}\mathrm{d}x \\
=&\int_{A\setminus B(G^{-1}h(t),\rho)} |x - G^{-1}h(t)|^{-s}\mathrm{d}x - \int_{B(G^{-1}h(t),\rho)\setminus A} |x - G^{-1}h(t)|^{-s}\mathrm{d}x \\
\le&|A\setminus B(G^{-1}h(t),\rho)|\rho^{-s} - |B(G^{-1}h(t),\rho)\setminus A|\rho^{-s} = 0.
\end{aligned}$$

Consequently,

$$\int_A |x - G^{-1}h(t)|^{-s}\mathrm{d}x \le \int_{B(G^{-1}h(t),\rho)} |x - G^{-1}h(t)|^{-s}\mathrm{d}x. \tag{3.5}$$

By the choice of γ, $s := (\frac{d}{2} - \frac{1}{q})(1-\gamma)^{-1} = d\frac{p-1}{p(1-\gamma)} < d$. Thus, in view of the inequality $|Gx - h(t)| \ge \|G^{-1}\|^{-1}|x - G^{-1}h(t)|$, together with (3.5), changing to polar coordinates leads to

$$\begin{aligned}
\int_A |Gx - h(t)|^{-s}\mathrm{d}x \le&\|G^{-1}\|^s \int_{B(G^{-1}h(t),\rho)} |x - G^{-1}h(t)|^{-s}\mathrm{d}x \\
\le&\|G^{-1}\|^s|\mathbb{S}^{d-1}| \int_0^\rho r^{-s}r^{d-1}\mathrm{d}r \\
\le&\|G^{-1}\|^s|\mathbb{S}^{d-1}|\frac{p(1-\gamma)}{d(1-p\gamma)}\rho^{d\frac{1-p\gamma}{p(1-\gamma)}}.
\end{aligned}$$

Therefore, with the identity $|A| = |\mathbb{S}^{d-1}|\rho^d$, we arrive at

$$\int_A |Gx - h(t)|^{-s}\mathrm{d}x \le C(s,d,\gamma,p)|A|^{\frac{1-p\gamma}{p(1-\gamma)}}.$$

with a constant $C(s,d,\gamma,p) = \|G^{-1}\|^s|\mathbb{S}^{d-1}|^{\frac{p-1}{p(1-\gamma)}}\frac{p(1-\gamma)}{d(1-p\gamma)}$. This and (3.4) imply

$$\|\mathcal{S}\chi_A\|_{L^{q,\infty}(I)} \le C(s,d,\gamma,p)^{1-\gamma}|A|^{\frac{1}{p}-\gamma}\Big\|\Big(\int_A |Gx - h(t)|^{-\frac{1}{q\gamma}}\mathrm{d}x\Big)^\gamma\Big\|_{L^{q,\infty}(I)}. \tag{3.6}$$

It remains to estimate the last term in (3.6). Actually, by definition,

$$\begin{aligned}
\Big\|\Big(\int_A |Gx - h(t)|^{-\frac{1}{q\gamma}}\mathrm{d}x\Big)^\gamma\Big\|_{L^{q,\infty}(I)} =& \Big(\Big\|\int_A |Gx - h(t)|^{-\frac{1}{q\gamma}}\mathrm{d}x\Big\|_{L^{q\gamma,\infty}(I)}\Big)^\gamma \\
\le& \Big(\int_A \Big\||Gx - h(t)|^{-\frac{1}{q\gamma}}\Big\|_{L^{q\gamma,\infty}(I)}\mathrm{d}x\Big)^\gamma \\
=& \Big(\int_A \Big\||Gx - h(t)|^{-1}\Big\|^{\frac{1}{q\gamma}}_{L^{1,\infty}(I)}\mathrm{d}x\Big)^\gamma.
\end{aligned} \tag{3.7}$$

Next we fix any $x \in A$, and estimate $\big\||Gx - h(t)|^{-1}\big\|_{L^{1,\infty}(I)}$. Let $g(t) := |Gx - h(t)|^{-1}$. Then, under Assumption 3.1, the nonincreasing rearrangement function $g^*(\tau)$ for $\tau \ge 0$ can be bounded by

$$g^*(\tau) \le 2C_h N_h \tau^{-1}, \tag{3.8}$$

where the rearrangement function $g^*(\tau)$ is defined by

$$\begin{aligned}
g^*(\tau) &= \inf\{c : \big|\{t : |g(t)| \ge c\}\big| \le \tau\} \\
&= \inf\{c : \big|\{t : |h(t) - Gx| \le c^{-1}\}\big| \le \tau\},
\end{aligned}$$

by slightly abusing the notation $|\cdot|$ for the Lebesgue measure of a set. Indeed, we have the trivial inclusion $\{t : |h(t) - Gx| \le c^{-1}\} \subset \cup_{j=1}^{N_x}\{t \in [\max(0, t_{j-1}), \min(t_{j+1}, T)] : |h(t) - h(t_j)| \le c^{-1}\}$, where the time instances t_j satisfy $h(t_j) = Gx$, for $j = 1, \ldots, N_x \le N_h$, under Assumption 3.1. Further, for any $t \in [t_{j-1}, t_j]$, by the mean value theorem, there exists some $\xi_j \in [t_{j-1}, t_j]$ such that $|h(t) - h(t_j)| = |\dot{h}(\xi_j)(t - t_j)|$, then the assertion (3.8) follows. Consequently

$$\big\||Gx - h(t)|^{-1}\big\|_{L^{1,\infty}(I)} := \sup_{\tau>0} \tau g^*(\tau) \le 2C_h N_h.$$

Now plugging this into (3.7) yields

$$\Big\|\Big(\int_A |Gx - h(t)|^{-\frac{1}{q\gamma}} \mathrm{d}x\Big)^{\gamma}\Big\|_{L^{q,\infty}(I)} \le (2C_h N_h)^{\frac{1}{q}} |A|^{\gamma},$$

which, together with (3.6), directly implies

$$\|\mathcal{S}\chi_A\|_{L^{q,\infty}(I)} \le (2C_h N_h)^{\frac{1}{q}} C(s, d, \gamma, p)^{1-\gamma} |A|^{\frac{1}{p}}.$$

Upon letting $\gamma = \frac{p+q}{2pq}$, we obtain the desired estimate. This completes the proof of the lemma. □

The next lemma shows that the operator $\mathcal{R} : L^q(D) \to L^2(D)$ is compact, for any $q > \frac{2(d-1)}{d}$.

Lemma 3.3. *Under the conditions of Lemma 3.2, for any $q > \min(1, \frac{2(d-1)}{d})$, $\mathcal{R}$ extends to a compact operator from $L^q(D)$ to $L^2(D)$. Especially, $\mathcal{R}$ is compact on $L^2(D)$.*

Proof. This follows directly from Lemma 3.2 and a duality argument. □

By Lemma 3.3, the operator $\mathcal{R}$ is nonnegative, compact and self-adjoint on $L^2(D)$. By spectral theory for compact operators [46], it has at most countably many discrete eigenvalues, with zero being the only accumulation point, and each nonzero eigenvalue has only finite multiplicity. Let $\{\lambda_n\}_{n=1}^{\infty}$ be the sequence of eigenvalues (with multiplicity counted) associated to $\mathcal{R}$, which are ordered nonincreasingly, and $\{\phi_n\}_{n=1}^{\infty}$ the corresponding eigenfunctions (orthonormal in $L^2(D)$). Moreover, spectral theory implies

$$\forall v \in L^2(D): \quad \mathcal{R}v = \sum_{n=1}^{\infty} \lambda_n (v, \phi_n)\phi_n, \tag{3.9}$$

with $(\cdot, \cdot)$ being the $L^2(D)$ inner product. Let $q^* = \infty$ for $d = 2$, and $q^* = 4$ for $d = 3$. Then by Lemma 3.2 and [29, Theorem 5.4, p. 83], the eigenfunctions $\{\phi_n\}_{n=1}^{\infty}$ have the following summability: For any $q < q^*$ and any $n \in \mathbb{N}_+$, $\phi_n \in L^q(D)$. This and the spectral decomposition (3.9) imply that the spectrum of the operator $\mathcal{R}$ will not change if its domain is restricted to $L^{2+\epsilon}(D)$ for any $0 < \epsilon < 1$.

Now we extend Theorem 3.2 to the kernel $|Gx - h(t)|^{-\frac{d}{2}}$. This result will be used in Section 4.2. We need a few concepts from spectral theory in Banach spaces [37]. Given two Banach spaces E and F, the n-th approximation number $a_n(W)$ and the Weyl number $x_n(W)$ of an operator $W \in \mathcal{B}(E, F)$ (i.e., the set of all bounded linear operators from E to F) are defined by

$$a_n(W) := \inf\{\|W - L\|_{\mathcal{B}(E,F)} : L \in \mathfrak{F}(E, F),\ \mathrm{rank}(L) < n\},$$

and

$$x_n(W) := \sup\{a_n(WX) : X \in \mathcal{B}(\ell_2, E), \|X\|_{\mathcal{B}(\ell_2,E)} \le 1\},$$

respectively, where $\mathfrak{F}(E, F)$ denotes the set of the finite rank operators and WX is the product of the two operators W and X. Furthermore, the following multiplicative property on Weyl numbers holds [37, Sections 2.4 and 3.6.2]:

Proposition 3.1. *For all $n \in \mathbb{N}_+$, $X \in \mathcal{B}(E_0, E)$, $W \in \mathcal{B}(E, F)$ and $Y \in \mathcal{B}(F, F_0)$, there holds*

$$x_n(YWX) \le \|Y\|_{\mathcal{B}(F,F_0)} x_n(W) \|X\|_{\mathcal{B}(E_0,E)}.$$

Theorem 3.3. *Let Assumption 3.1 hold, and* $f(x,t) := |Gx - h(t)|^{-\frac{d}{2}}$ *with* $d = 2, 3$. *Then* $\lambda_n \leq Cn^{-\frac{1}{2}+\epsilon}$ *as* $n \to \infty$ *for any* $\epsilon > 0$.

Proof. Let $\widetilde{\mathcal{S}} := \mathcal{S}|_{L^{2+\epsilon}(D)}$ for some small fixed $\epsilon > 0$, i.e., the restriction of $\mathcal{S}$ on $L^{2+\epsilon}(D)$. Then by Lemma 3.2(i), the range of $\mathcal{S}$ is $L^\infty(I)$. Hence, we can decompose $\widetilde{S} : L^{2+\epsilon}(D) \to L^{2+\epsilon}(I)$ into $\widetilde{\mathcal{S}} = \mathcal{I}\widetilde{\mathcal{S}}$, where $\mathcal{I}$ is the embedding operator from $L^\infty(I)$ to $L^{2+\epsilon}(I)$. The multiplicative property of Weyl numbers x_n in Proposition 3.1 implies

$$x_n(\mathcal{I}\tilde{\mathcal{S}}) \leq x_n(\mathcal{I})\|\tilde{\mathcal{S}}\|_{\mathcal{B}(L^{2+\epsilon}(D),L^\infty(I))}.$$

By [37, Section 6.3.4, p. 250], there holds $x_n(\mathcal{I}) \leq Cn^{-\frac{1}{2+\epsilon}}$. Thus, we arrive at

$$x_n(\mathcal{I}\tilde{\mathcal{S}}) \leq Cn^{-\frac{1}{2+\epsilon}}.$$

Meanwhile, Lemma 3.2(ii) and a standard duality argument indicate that the dual operator $\mathcal{S}^*$ is bounded from $L^{2+\epsilon}(I)$ to $L^{2+\epsilon}(D)$. Note that $\widetilde{\mathcal{R}} = \mathcal{R}|_{L^{2+\epsilon}(D)}$, and its eigenvalues are $\{\lambda_n\}_{n=1}^\infty$, which can be bounded by the Weyl numbers $x_n(\widetilde{\mathcal{R}})$ according to the eigenvalue theorem for Weyl operators [37, Section 3.6.2]. Hence, we deduce

$$\lambda_n \leq Cx_n(\widetilde{\mathcal{R}}) = Cx_n(\mathcal{S}^*\mathcal{I}\tilde{\mathcal{S}}) \leq C\|\mathcal{S}^*\|_{\mathcal{B}(L^{2+\epsilon}(I),L^{2+\epsilon}(D))}x_n(\mathcal{I}\tilde{\mathcal{S}}).$$

where the last step is due to Proposition 3.1. Combining the preceding estimates completes the proof. □

Remark 3.2. *The bound in Theorem 3.3 seems not sharp. The sharp one is conjectured to be* $O(n^{-1+\epsilon})$. *The statement remains valid if the kernel* $f(x,t)$ *is multiplied by a bounded function. This fact will be used below in Section 4.2.*

4 Degree of ill-posedness

Now we analyze the degree of ill-posedness of the equilibrium MPI model (2.6) via the SV decay rate of the associated integral operator, and focus on three cases: (a) nonfiltered equilibrium model, (b) limit model, and (c) filtered equilibrium model. Dependent of the problem setting, the behavior of the forward operator can differ substantially [43]. Our analysis below sheds insights into these observations. Since the experimental parameters for all the receive coils are comparable in practice, our analysis below focuses on one receive coil, which allows us to simplify the notation. The decay rate given below only determines the best possible degree of ill-posedness (i.e., upper bounds on SVs), and the results should be only used as an indicator of the degree of ill-posedness.

4.1 The non-filtered equilibrium model

First, we consider the case in the absence of the temporal analog filter $a(t)$, and discuss the influence of the filter in Section 4.3 below. Then the MPI forward operator $F : L^2(\Omega) \to L^2(I)$ is given by

$$\begin{cases} v(t) = \displaystyle\int_\Omega c(x)\kappa(x,t)\mathrm{d}x, \\ \kappa = \mu_0 m_0 p^t \dfrac{\mathrm{d}}{\mathrm{d}t}\left[\dfrac{\mathcal{L}_\beta(|H|)}{|H|}H\right], \\ H(x,t) = g(x) - h(t). \end{cases} \tag{4.1}$$

Now we can state our first main result.

Theorem 4.1. *Let* $0 < \beta < \infty$, $d = 1, 2, 3$, $h \in (H^s(I))^d$ *with* $s \geq 1$, $g \in (L^\infty(\Omega))^d$, *and* $p \in (L^\infty(\Omega))^d$. *Then for the operator* $F : L^2(\Omega) \to L^2(I)$ *defined in* (4.1), *the SVs* σ_n *decay as* $\sigma_n \leq Cn^{\frac{1}{2}-s}$.

Proof. Since $h \in (H^s(I))^d$ and $g \in (L^\infty(\Omega))^d$, by Sobolev embedding, the function $H(x,t) = g(x) - h(t) \in H^s(I;(L^\infty(\Omega))^d) \subset L^\infty(I;(L^\infty(\Omega))^d)$, and $\dot{H}(x,t) = -\dot{h}(t) \in (H^{s-1}(I))^d$. Clearly, we have

$$p^t H \in H^s(I;L^\infty(\Omega)) \quad \text{and} \quad p^t \dot{H} = -p^t \dot{h} \in H^{s-1}(I;L^\infty(\Omega)). \tag{4.2}$$

Further, by Lemma 2.1, $\frac{L_\beta(\sqrt{z})}{\sqrt{z}} \in C_B^\infty([0,\infty))$ and since $s \geq 1$, by Theorem 3.1, simple computation shows $|H|^2 \in H^s(I;L^\infty(\Omega))$, and thus by Lemma 3.1(i), $\frac{L_\beta(|H|)}{|H|} \in H^s(I;L^\infty(\Omega))$ and $\frac{\mathrm{d}}{\mathrm{d}t}\frac{L_\beta(|H|)}{|H|} \in H^{s-1}(I;L^\infty(\Omega))$. Now, by the product rule, (4.2) and Theorem 3.1, we deduce

$$\begin{aligned} \kappa &= \mu_0 m_0 p^t \frac{\mathrm{d}}{\mathrm{d}t}\left(\frac{L_\beta(|H|)}{|H|}H\right) \\ &= \mu_0 m_0 \left(p^t H \frac{\mathrm{d}}{\mathrm{d}t}\frac{L_\beta(|H|)}{|H|} + \frac{L_\beta(|H|)}{|H|} p^t \dot{H}\right) \\ &\in H^{s-1}(I;L^\infty(\Omega)) \subset H^{s-1}(I;L^2(\Omega)). \end{aligned} \tag{4.3}$$

Then the desired assertion follows from Theorem 3.2. □

Remark 4.1. *For $p, g \in (L^\infty(\Omega))^d$, Theorem 4.1 describes the potential influence of the trajectory $h(t)$ on the SV decay. For smooth trajectories, i.e., $h(t) \in (C^\infty(I))^d$ (e.g., sinusoidal trajectory, common in experimental setup), the SVs decay rapidly, and thus the inverse problem is very ill-posed. For nonsmooth trajectories, i.e., triangular trajectory ($h(t) \in (H^{\frac{3}{2}-\epsilon}(I))^d$, for any $\epsilon \in (0, \frac{1}{2})$), the decay may be slower.*

In Theorem 4.1, we assume $p, g \in (L^\infty(\Omega))^d$ only. It does not account for possible additional regularity of $\kappa(x,t)$ in the spatial variable x. In practice, it is often taken to be homogeneous/linear, and thus $\kappa(x,t)$ is very smooth in x. This extra regularity can significantly affect the SV decay, which is described next.

Theorem 4.2. *Let $0 < \beta < \infty$, $d = 1,2,3$, $h \in (H^s(I))^d$ with $s > \frac{3}{2}$, $g \in (H^r(\Omega))^d$, $r > \frac{d}{2}$ and $p \in (C^\infty(\Omega))^d$. Then for the operator $F : L^2(\Omega) \to L^2(I)$ defined in (4.1), the SVs σ_n decay as $\sigma_n \leq Cn^{-\frac{1}{2}-\frac{r}{d}}$.*

Proof. By Sobolev embedding, for $s > \frac{3}{2}$, $\dot{H}(x,t) = -\dot{h}(t) \in (H^{s-1}(I))^d \subset (L^\infty(I))^d$. Then under the given assumptions, $H(x,t) = g(x) - h(t) \in H^r(\Omega;(H^s(I))^d) \subset H^r(\Omega;(W^{1,\infty}(I))^d) \subset L^\infty(\Omega;(W^{1,\infty}(I))^d)$. By Lemma 2.1, $\frac{L_\beta(\sqrt{z})}{\sqrt{z}} \in C_B^\infty([0,\infty))$, and by Theorem 3.1, we deduce $|H(x,t)|^2 \in H^r(\Omega;W^{1,\infty}(I))$. Hence, Lemma 3.1(ii) implies $\frac{L_\beta(|H(x,t)|)}{|H(x,t)|} \in H^r(\Omega;W^{1,\infty}(I))$, and $\frac{\mathrm{d}}{\mathrm{d}t}\frac{L_\beta(|H(x,t)|)}{|H(x,t)|} \in H^r(\Omega;L^\infty(I))$. Further, for $r > \frac{d}{2}$, for small $\epsilon > 0$, we have $2r - \frac{d}{2} - \epsilon > r$, and thus it follows from (4.2) and Theorem 3.1 that $p^t H \frac{\mathrm{d}}{\mathrm{d}t}\frac{L_\beta(|H(x,t)|)}{|H(x,t)|} \in H^r(\Omega;L^\infty(I))$ and similarly $\frac{L_\beta(|H(x,t)|)}{|H(x,t)|} p^t \dot{h}(t) \in H^r(\Omega;L^\infty(I))$. These two inclusions and (4.3) show that $\kappa \in H^r(\Omega;L^\infty(I)) \subset H^r(\Omega;L^2(I))$. Thus, by Theorem 3.2, the SVs of the adjoint operator decay as $O(n^{-\frac{1}{2}-\frac{r}{d}})$. Since the adjoint operator $F^* : L^2(I) \to L^2(\Omega)$(with respect to the $L^2(I \times \Omega)$ inner product) shares the SVs [12, p. 27, eq. (2.1)], the desired assertion follows. □

By Theorem 4.2, the SVs can decay fast for a nonsmooth trajectory $h(t)$, so long as $p(x)$ and $g(x)$ are sufficiently smooth. The regularity requirement might be relaxed by analyzing more precisely pointwise multiplication in Bochner-Sobolev spaces. Since $\dot{h}(t)$ and $p(x)$ enter the kernel $\kappa(x,t)$ as pointwise multipliers, if uniformly bounded, they act as bounded operators on $L^2(I)$ and $L^2(\Omega)$, respectively, and the decay rate remains valid [12, p. 27, eq. (2.2)].

4.2 Limit model

It was reported that the spatial resolution increases with particle diameter D [43, 23], i.e., a large β value in the model (4.1). Hence, we analyze the limit case $\beta \to \infty$ below. First, we derive the expression for the limit integral operator. Throughout this part, in Assumption 3.1, the domain D refers to Ω.

Proposition 4.1. *Let $h \in (H^s(I))^d$ with $s \geq 1$, $g \in (L^\infty(\Omega))^d$, and $p \in (L^\infty(\Omega))^d$. For $\beta \to \infty$, there holds*

$$\frac{\mathrm{d}}{\mathrm{d}t}\left(\mu_0 p^t L_\beta(|H|)\frac{H}{|H|}\right) \to \frac{\mathrm{d}}{\mathrm{d}t}\left(\mu_0 p^t \frac{H}{|H|}\right) \quad \text{in } H^{-1}(I;L^2(\Omega)),$$

and the limit integral operator $\widetilde{F}$ *of the operator* F *defined in* (4.1) *is given by*

$$\begin{cases} v(t) = \displaystyle\int_\Omega c(x)\tilde{\kappa}(x,t)\mathrm{d}x, \\ \tilde{\kappa} = \mu_0 m_0 p^t \left(-\dfrac{HH^t}{|H|^3} + \dfrac{1}{|H|} I_d\right) \dot{H}, \\ H(x,t) = g(x) - h(t). \end{cases} \tag{4.4}$$

Proof. First, by the assumptions on g, h and p and Sobolev embedding theorem, $H(x,t) = g(x) - h(t) \in (L^\infty(\Omega \times I))^d$. Then for any $\phi(t) \in H_0^1(I)$ and $\psi(x) \in L^2(\Omega)$, integration by parts yields

$$\begin{aligned} &\int_I \int_\Omega \mu_0 m_0 p(x)^t \frac{\mathrm{d}}{\mathrm{d}t} \left[L_\beta(|H(x,t)|) \frac{H(x,t)}{|H(x,t)|} \right] \phi(t)\psi(x)\mathrm{d}x\mathrm{d}t \\ =& - \int_I \int_\Omega \mu_0 m_0 p(x)^t L_\beta(|H(x,t)|) \frac{H(x,t)}{|H(x,t)|} \dot{\phi}(t)\psi(x)\mathrm{d}x\mathrm{d}t. \end{aligned}$$

Now it follows from Cauchy-Schwarz inequality that

$$\begin{aligned} &\Big| \int_I \int_\Omega [L_\beta(|H(x,t)|) - \mathrm{sign}(|H(x,t)|)] \mu_0 m_0 p(x)^t \frac{H(x,t)}{|H(x,t)|} \dot{\phi}(t)\psi(x)\mathrm{d}x\mathrm{d}t \Big| \\ \le& \mu_0 m_0 \|p\|_{(L^\infty(\Omega))^d} \int_I \int_\Omega \Big| L_\beta(|H(x,t)|) - \mathrm{sign}(|H(x,t)|) \Big| \times |\dot{\phi}(t)\psi(x)| \mathrm{d}x\mathrm{d}t \\ \le& \mu_0 m_0 \|p\|_{(L^\infty(\Omega))^d} \Big\| L_\beta(|H(x,t)|) - \mathrm{sign}(|H(x,t)|) \Big\|_{L^2(\Omega\times I)} \|\dot{\phi}\|_{L^2(I)} \|\psi\|_{L^2(\Omega)}. \end{aligned}$$

Since $\|H\|_{L^\infty(\Omega\times I)} < \infty$, by Lemma 2.1(i) and Lebesgue's dominated convergence theorem, we deduce

$$\lim_{\beta\to\infty} \|L_\beta(|H(x,t)|) - \mathrm{sign}(|H(x,t)|)\|_{L^2(\Omega\times I)} = 0.$$

By integration by parts again, and density of the product $\psi\phi$ in $H_0^1(I; L^2(\Omega)) \simeq L^2(\Omega; H_0^1(I))$ (see, e.g., [37, Section 6.2, p. 244] or [18, Lemma 1.2.19, p. 23]), we obtain the assertion. □

Next we analyze the decay rate of the SVs of the limit operator $\widetilde{F}$. First, we give a result on the Bochner-Sobolev regularity of the function $|Gx - h(t)|^r$, $r > -\frac{d}{2}$.

Lemma 4.1. *Let Assumption 3.1 hold, and let* $h(t)$ *be sufficiently smooth. Then for any* $r > -\frac{d}{2}$*, the function* $f(x,t) = |Gx - h(t)|^r \in H^s(I; L^2(\Omega))$ *for any* $s < r + \frac{d}{2}$.

Proof. Let $\epsilon > 0$ be sufficiently small and $r = -\frac{d}{2} + \frac{\epsilon}{2}$. Since G is invertible, by the relation $|Gx - h(t)| = |G(x - G^{-1}h(t))| \ge \|G^{-1}\|^{-1}|x - G^{-1}h(t)|$ for any fixed $t \in [0,T]$, we have

$$\int_I \int_\Omega |Gx - h(t)|^{-d+\epsilon} \mathrm{d}x\mathrm{d}t \le \|G^{-1}\|^{d-\epsilon} \int_0^T \Big(\int_\Omega |x - G^{-1}h(t)|^{-d+\epsilon} \mathrm{d}x \Big) \mathrm{d}t.$$

Let $B(G^{-1}h(t), \rho) := \{x \in \mathbb{R}^d : |x - G^{-1}h(t)| \le \rho\}$ satisfy that $|B(G^{-1}h(t), \rho)| = |\Omega|$, which implies $|\Omega| = |\mathbb{S}^{d-1}|\rho^d$. By (3.5) with $A := \Omega$, we obtain

$$\int_I \int_\Omega |Gx - h(t)|^{-d+\epsilon} \mathrm{d}x\mathrm{d}t \le \|G^{-1}\|^{d-\epsilon} \int_0^T \Big(\int_{B(G^{-1}h(t),\rho)} |x - G^{-1}h(t)|^{-d+\epsilon} \mathrm{d}x \Big) \mathrm{d}t.$$

Then changing to polar coordinates for the inner integral leads to

$$\begin{aligned} \int_I \int_\Omega |Gx - h(t)|^{-d+\epsilon} \mathrm{d}x\mathrm{d}t &\le \|G^{-1}\|^{d-\epsilon} T \int_0^\rho r^{-d+\epsilon} r^{d-1} \mathrm{d}r |\mathbb{S}^{d-1}| \\ &= \epsilon^{-1} \|G^{-1}\|^{d-\epsilon} T |\Omega|^{\frac{\epsilon}{d}} |\mathbb{S}^{d-1}|^{1-\frac{\epsilon}{d}}. \end{aligned} \tag{4.5}$$

This proves $f(x,t) \in L^2(I;L^2(\Omega))$ for all $r > -\frac{d}{2}$. Next, the derivative $\dot f$ of $f = |Gx - h(t)|^r$ is given by $\dot f = -r|Gx-h(t)|^{r-2}(Gx-h(t))^t\dot h(t)$. Thus, $|\dot f| \le r|Gx-h(t)|^{r-1}|\dot h(t)|$, which, together with (4.5), implies that for $r = -\frac{d}{2} + 1 + \frac{\epsilon}{2}$, there holds

$$\|\dot f\|_{L^2(I;L^2(\Omega))} \le r\sqrt{\epsilon^{-1}\|G^{-1}\|^{d-\epsilon}T|\Omega|^{\frac{\epsilon}{d}}|\mathbb{S}^{d-1}|^{1-\frac{\epsilon}{d}}}\|\dot h\|_{L^2(I)}.$$

Thus, $\|f\|_{H^1(I;L^2(\Omega))} < \infty$. By interpolation, for any $-\frac{d}{2} + \frac{\epsilon}{2} < r < -\frac{d}{2} + 1 + \frac{\epsilon}{2}$, there holds $|Gx - h(t)|^r \in H^r(I;L^2(\Omega))$, with $s = r + \frac{d}{2}$. The general case of any $r > -\frac{d}{2} + 1$ can be analyzed analogously. The desired assertion follows since the constant $\epsilon \in (0, \frac{1}{2})$ can be made arbitrarily small. □

Lemma 4.1 does not cover the case $r = -\frac{d}{2}$, which is treated next.

Lemma 4.2. *Let Assumption 3.1 hold. Then for any $p \in (1,2)$, the function $f(x,t) = |Gx - h(t)|^{-\frac{d}{2}} \in L^{2-\epsilon}(\Omega;L^p(I))$ for any $\epsilon > 0$.*

Proof. We only need to show

$$g(x) := \int_I |Gx - h(t)|^{-\frac{pd}{2}}\,\mathrm{d}t \in L^{\frac{2}{p},\infty}(\Omega) \quad \text{ for all } p \in (1,2). \tag{4.6}$$

Note that $L^{2,\infty}(\Omega) \subset L^{2-\epsilon}(\Omega)$ for all $\epsilon > 0$ [10, Section 6.4], and hence, $f(x,t) \in L^{2-\epsilon}(\Omega;L^p(I))$ for any $p \in (1,2)$. Next we prove (4.6). Since $L^{\frac{2}{p},\infty}(\Omega)$ is a Banach space with a well-defined norm, we deduce

$$\|g\|_{L^{\frac{2}{p},\infty}(\Omega)} = \Big\|\int_I |Gx - h(t)|^{-\frac{pd}{2}}\,\mathrm{d}t\Big\|_{L^{\frac{2}{p},\infty}(\Omega)} \le \int_I \Big\||Gx - h(t)|^{-\frac{pd}{2}}\Big\|_{L^{\frac{2}{p},\infty}(\Omega)}\mathrm{d}t. \tag{4.7}$$

Let $w(x,t) := |Gx - h(t)|^{-\frac{pd}{2}}$. To estimate $\|g\|_{L^{\frac{2}{p},\infty}(\Omega)}$, we first compute the nonincreasing rearrangement $w^*(\tau,t)$ for any fixed $t \in I$, which, by definition, is defined for all $\tau \ge 0$ by

$$\begin{aligned} w^*(\tau,t) &= \inf\{c > 0 : |\{x \in \Omega : w(x,t) > c\}| \le \tau\} \\ &= \inf\{c > 0 : |\{x \in \Omega : |Gx - h(t)| < c^{-\frac{2}{pd}}\}| \le \tau\}. \end{aligned}$$

This and the inclusion relation $\{x \in \Omega : |Gx - h(t)| < c^{-\frac{2}{pd}}\} \subset \{x \in \Omega : |x - G^{-1}h(t)| < \|G^{-1}\|c^{-\frac{2}{pd}}\}$ (due to the trivial inequality $|Gx - h(t)| \ge \|G^{-1}\|^{-1}|x - G^{-1}h(t)|$) yield

$$w^*(\tau,t) \le \Big(|\mathbb{S}^{d-1}|\|G^{-1}\|^d\tau^{-1}\Big)^{\frac{p}{2}}.$$

Hence, for any fixed $t \in I$, we obtain

$$\begin{aligned} \Big\||Gx - h(t)|^{-\frac{pd}{2}}\Big\|_{L^{\frac{2}{p},\infty}(\Omega)} = \|w(x,t)\|_{L^{\frac{2}{p},\infty}(\Omega)} &\le \sup_{\tau\ge 0}\tau^{\frac{p}{2}}\Big(|\mathbb{S}^{d-1}|\|G^{-1}\|^d\tau^{-1}\Big)^{\frac{p}{2}} \\ &= \Big(|\mathbb{S}^{d-1}|\|G^{-1}\|^d\Big)^{\frac{p}{2}}, \end{aligned}$$

which, in view of (4.7), yields (4.6). This completes the proof of the lemma. □

Now we can state the degree of ill-posedness for the limit problem for FFP trajectories.

Theorem 4.3. *For $\beta \to \infty$, if $p \in (L^\infty(\Omega))^d$, $h \in (H^s(I))^d$ with $s > \frac{3}{2}$, $d = 2,3$, for FFP trajectories, the SVs σ_n of the operator $\widetilde F$ defined in (4.4) decay as (for any $\epsilon \in (0, \frac{1}{4})$):*

$$\sigma_n \le \begin{cases} Cn^{-1+\epsilon}, & d = 3, \\ Cn^{-\frac{1}{4}+\epsilon}, & d = 2. \end{cases}$$

Proof. By the Cauchy-Schwarz inequality, there holds $|\tilde{\kappa}| \leq \mu_0 m_0 |p||H|^{-1}|\dot{H}|$. Now we discuss the cases $d = 2$ and $d = 3$ separately. For $d = 3$, by Lemma 4.1, $|H|^{-1} \in H^{\frac{1}{2}-\epsilon}(I; L^2(\Omega))$, and since $s > \frac{3}{2}$, by Sobolev embedding, $\dot{H} = -\dot{h} \in (H^{s-1}(I))^3 \subset (L^\infty(I))^3$. By Theorem 3.1 and $p \in (L^\infty(\Omega))^3$, we have $|H|^{-1}|\dot{h}| \in H^{\frac{1}{2}-\epsilon}(I; L^2(\Omega))$. Then the assertion follows from Theorem 3.2. The case $d = 2$ is similar: since $|\dot{h}| \in L^\infty(I)$ and $|p| \in L^\infty(\Omega)$, we apply Theorem 3.3 to obtain the desired assertion. □

In practice, one can also have FFL trajectories for $d = 3$, where $G \in \mathbb{R}^{3\times 3}$ has only rank 2. Then for any fixed $t \in I$, the kernel function $\tilde{\kappa}(x, t)$ is singular along a line in Ω, instead of at one single point. We analyze a simplified model to gain insight. Since $\operatorname{rank}(G) = 2$ and symmetric, by properly changing the coordinate, we may assume that G is diagonal with the last diagonal entry being zero. Then the condition for any fixed $t \in I$, there exists $x \in \Omega$ such that $Gx = h(t)$ implies $h_3(t) = 0$, and the singular kernel essentially depends only on $h_1(t)$ and $h_2(t)$, and the third component of $H(x, t)$ vanishes. Thus for a cylindrical domain $\Omega = \Omega_{12} \times \Omega_3$, the forward operator $\tilde{F}$ can be reformulated as in the 2D FFP trajectories (with respect to the average $\int_{\Omega_3} c(x)\mathrm{d}x_3$ of the concentration $c(x)$):

$$v(t) = -\mu_0 m_0 \int_{\Omega_{12}} \Big(\int_{\Omega_3} c(x)\mathrm{d}x_3 \Big) p(x)^t \left(-\frac{HH^t}{|H|^3} + \frac{1}{|H|} I_3 \right) \dot{H}\mathrm{d}x_1\mathrm{d}x_2.$$

The next result analyzes the degree of ill-posedness of FFL trajectories under the designate conditions.

Theorem 4.4. *Under the preceding assumptions, for $\beta \to \infty$, for FFL trajectories in 3D, $p \in (L^\infty(\Omega))^3$, and $h(t) \in (H^s(I))^3$ with $s > \frac{3}{2}$, the SVs σ_n of the operator $\widetilde{F}$ decay as $\sigma_n \leq Cn^{-\frac{1}{4}+\epsilon}$, for any $\epsilon \in (0, \frac{1}{4})$.*

Proof. The proof is similar to Theorem 4.3 with $d = 2$. Since $s > \frac{3}{2}$, by Sobolev embedding, $\dot{H} = -\dot{h}(t) \in (H^{s-1}(I))^3 \hookrightarrow (L^\infty(I))^3$. Since the third component of H vanishes, this and Theorem 3.3 yield the assertion. □

Remark 4.2. *In Theorems 4.3 and 4.4, the trajectory $h(t)$ is assumed to be $(H^s(I))^d$, with $s > \frac{3}{2}$. This restriction comes from the requirement $\dot{h}(t) \in (L^\infty(I))^d$ to simplify the analysis. The estimates in Theorem 4.4 and Theorem 4.3 for $d = 2$ are conservative, due to suboptimal bound in Theorem 3.3 (see Remark 3.2).*

4.3 Filtered model

In practice, the signal is first preprocessed by an analog filter to remove the excitation so that the true signal is not lost during digitalization. This can be achieved by a band stop filter. Mathematically, it amounts to convolution with a given kernel $a(t) : \bar{I} := [-T, T] \to \mathbb{R}$ defined by

$$\widehat{\kappa}(x, t) = \int_I \kappa(x, t')a(t - t')\mathrm{d}t' \quad \forall t \in I. \tag{4.8}$$

However, the precise form of the filter $a(t)$ remains elusive, which currently constitutes one of the major challenges in realistic mathematical modeling of MPI [21]. To analyze the influence of the filtering step, we recall a smoothing property of the convolution operator [5, Theorem 3]. Below the notation $(\cdot)_+$ denotes the positive part. We refer to [41] for a treatise on Besov spaces $B^s_{p,\theta}(\mathbb{R})$.

Lemma 4.3. *For $-\infty < \ell_1, \ell_2 < \infty$, $1 \leq p_1 \leq p_2 \leq \infty$, $0 < \theta_1, \theta_2 \leq \infty$, with $\frac{1}{p} = \frac{1}{p_1'} + \frac{1}{p_2}$ and $\frac{1}{\theta} \geq (\frac{1}{\theta_2} - \frac{1}{\theta_1})_+$, then for $f \in B^{\ell_2-\ell_1}_{p,\theta}(\mathbb{R})$ and $g \in B^{\ell_1}_{p_1,\theta_1}(\mathbb{R})$, the convolution $f * g$ exists and*

$$\|f * g\|_{B^{\ell_2}_{p_2,\theta_2}(\mathbb{R})} \leq C\|f\|_{B^{\ell_2-\ell_1}_{p,\theta}(\mathbb{R})}\|g\|_{B^{\ell_1}_{p_1,\theta_1}(\mathbb{R})}.$$

Last, we describe the influence of filtering: the SVs σ_n of the filtered model decay faster than the nonfiltered one by a factor r, the regularity index of the filter.

Theorem 4.5. *Suppose that the zero extension of the filter $a(t) : \bar{I} \to \mathbb{R}$ belongs to $B^r_{1,\theta}(\mathbb{R})$, for some $r \geq 0$ and $0 < \theta \leq \infty$, and the conditions in Theorem 4.1 hold. Then the SVs σ_n of the operator $\widehat{F}$ for the kernel $\widehat{\kappa}(x, t)$ defined in (4.8) decay as $\sigma_n \leq Cn^{\frac{1}{2}-s-r}$.*

Proof. Let $\bar{\kappa}$ be any bounded extension of κ from $H^{s-1}(I;L^2(\Omega))$ to $H^{s-1}(\mathbb{R};L^2(\Omega))$, and denote by $\bar{a}$ the zero extension of $a : \bar{I} \to \mathbb{R}$ to $\mathbb{R} \setminus \bar{I}$. Then we can extend $\widehat{\kappa}$ from I to $\mathbb{R}$, still denoted by $\widehat{\kappa}$, by $\widehat{\kappa}(x,t) = \int_{\mathbb{R}} \bar{\kappa}(x,t')\bar{a}(t-t')\mathrm{d}t'$. Clearly, the restriction of $\widehat{\kappa}(x,t)$ to I coincides with $\widehat{\kappa}$ defined in (4.8), by the construction of the extension $\bar{a}$. This and the fact $H^s(\mathbb{R}) = B^s_{2,2}(\mathbb{R})$ [41, Remark 4, p. 179] imply

$$\begin{aligned}\|\widehat{\kappa}\|_{H^{s+r-1}(I;L^2(\Omega))} &= \|\bar{\kappa} * \bar{a}\|_{H^{s+r-1}(I;L^2(\Omega))} \le \|\bar{\kappa} * \bar{a}\|_{H^{s+r-1}(\mathbb{R};L^2(\Omega))} \\ &\le C\|\bar{\kappa}\|_{H^{s-1}(\mathbb{R};L^2(\Omega))}\|\bar{a}\|_{B^r_{1,\theta}(\mathbb{R})} \le C\|\kappa\|_{H^{s-1}(I;L^2(\Omega))}\|\bar{a}\|_{B^r_{1,\theta}(\mathbb{R})},\end{aligned}$$

where the second inequality is due to Lemma 4.3 and the last one due to the bounded extension. Then the assertion follows from Theorem 3.2. □

5 Numerical results

Now we illustrate the theoretical results with numerical examples for the non-filtered FFP and FFL cases. We do not study the influence of analog filter, since its mechanism and precise form are still poorly understood.

5.1 Setting of numerical experiments

In our numerical simulation, we use parameters that are comparable with real experiments. We parameterize problems (4.1) and (4.4) analogously to the Bruker FFP scanner, and obtain the parameter values from a public dataset [27]. Sinusoidal excitation patterns are used to move the FFP along Lissajous trajectories, which are often employed in practice due to its fast coverage of the domain of interest. In the FFP case, the gradient field $g : \mathbb{R}^3 \to \mathbb{R}^3$ is taken to be linear, i.e., $g(x) = Gx$ with $G \in \mathbb{R}^{3\times 3}$ diagonal and $\mathrm{trace}(G) = 0$. The drive field $h : I \to \mathbb{R}^3$ is taken to be trigonometric, i.e. $h(t) = -(A_1\sin(2\pi f_1 t), A_2\sin(2\pi f_2 t), A_3\sin(2\pi f_3 t))^t$, $A_i, f_i > 0$, $i = 1,2,3$. By Theorem 4.2, for $0 < \beta < \infty$, the good spatial regularity of the kernel $\kappa(x,t)$ precludes examining the influence of trajectory smoothness on the SV decay. Nonetheless, we consider also triangular trajectories, i.e., $h(t) = -(A_1\mathrm{tri}(2\pi f_1 t), A_2\mathrm{tri}(2\pi f_2 t), A_3\mathrm{tri}(2\pi f_3 t))^t$, $A_i, f_i > 0$, $i = 1,2,3$, where the function $\mathrm{tri} : \mathbb{R} \to [-1,1]$ is defined by

$$\mathrm{tri}(z) = \begin{cases} \frac{2}{\pi}\theta & \theta = (z \bmod 2\pi) \in [0, \pi/2), \\ 2 - \frac{2}{\pi}\theta & \theta = (z \bmod 2\pi) \in [\pi/2, 3\pi/2), \\ -4 + \frac{2}{\pi}\theta & \theta = (z \bmod 2\pi) \in [3\pi/2, \pi/2). \end{cases}$$

We refer to Fig. 1 for an illustration of Lissajous excitation with sinusoidal and triangular trajectories.

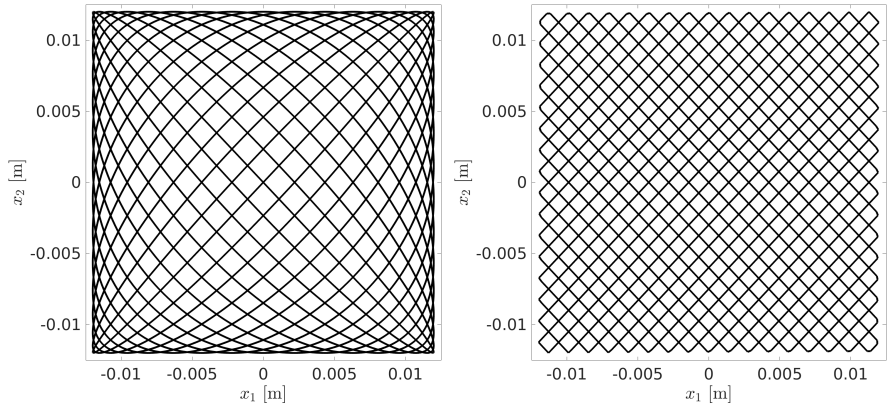

(a) sinusoidal (b) triangular

Figure 1: FFP trajecories Lissajous curve for sinusoidal (a) and triangular (b) excitation in 2D.

The scanner is equipped with three receive coil units, each sensitive to one component of the mean magnetic moment vector $\bar{m}(x,t)$. The coil sensitivities p are assumed to be homogeneous in the simulation.

The particle's magnetic moment m_0 is set to $m_0 = \mu_0^{-1}$ in order to avoid diameter-dependent numerical errors, and the remaining particle parameters are chosen following [6].

The forward operators F, $\tilde{F} : L^2(\Omega) \to (L^2(I))^L$ are discretized by a Galerkin method with piecewise constant basis functions on a rectangular partition of the spatial domain Ω and uniform partition of the time interval I. The integrals are computed using a quasi Monte-Carlo quadrature rule in the spatial variable x, with a Halton sequence with 3^d points, for which a good accuracy was reported [34]. It can also approximate singular integrals [36] arising in the limit case. The time integral is computed by a Gaussian quadrature rule, and interval splitting is performed if necessary such that discontinuities lie at the interval boundaries only. MATLAB's built-in function `svd` is used to compute SVs of the discrete model.

There are several sources of errors in computing SVs: discretization error of the integral operator, quadrature error by Gauss quadrature in time / quasi Monte Carlo method in space and possibly also numerical error with MATLAB function `svd` for computing matrix SVs. The first two sources seem dominant. The discretization error by the piecewise constant Galerkin method is of order $O(h)$, where h is the mesh size, if the integrand is smooth, and the quadrature error is analyzed for well behaved functions. In the nonfiltered model, the kernel function is well behaved, so existing theory may be applied. In the limit case, the kernel is highly singular, so one can only expect low-order convergence. A complete analysis of these errors is beyond the scope of the present work.

These observations indicate that one should not put a lot of confidence into the accuracy of the trailing part of small singular values and try to draw conclusions from this part, since these values are not reliably computed. In practice, researchers have been using leading SVs to determine the decay rate [13]; see also [48] for quantitative estimates on the percentage of reliable eigenvalues for the Laplacian by the Galerkin method (equivalently, SVs for the integral operator with Green's function as the kernel). The discussions below focus on leading SVs (note that the theoretical results hold for all n).

5.2 Numerical results and discussions

First, we compare the SV decays for the FFP case using sinusoidal excitation patterns moving the FFP along a Lissajous trajectory in the 2D and 3D cases. In all cases, for $d = 1, 2, 3$, the first d receive coils were used to compute the SVs. The parameters used in the numerical simulation are summarized in Table 1. In all the figures, the whole range of the SVs of the discrete problem is presented, where the small SVs are not reliable. The FFP results including the limit cases (2D/3D) are presented in Fig. 2, where for the purpose of comparison, the reference decay rates $O(n^{-\frac{1}{2}})$ and $O(n^{-1})$ are also shown. It is observed that as the particle diameter D increases, the decay rate approaches the theoretical one from Theorem 4.3, and for small D, the decay is exponential. The numerical results for the 2D FFP limit case agree well with the predictions from Theorem 4.3 and the conjecture in Remark 3.2. In the 3D FFP limit case, the decay of the leading SVs is slightly slower than the theoretical rate in Theorem 4.3. Similar observations hold for triangular excitations in the drive field and when using one single receive coil only. These results can be found in Figs. 3 and 4.

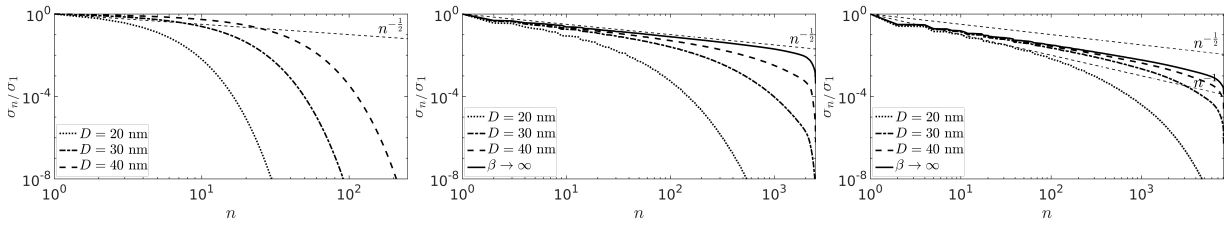

(a) FFP 1D (b) FFP 2D (c) FFP 3D

Figure 2: SV decay for sinusoidal excitation patterns and different particle diameters in (a) 1D, (b) 2D, and (c) 3D domains.

Next we consider the FFL case. We use a field free line in affine planes of the e_1-e_2-plane, following [25], where e_i denotes the ith canonical Cartesian coordinate. We use a dynamic selection field $g : \mathbb{R}^3 \times I \to \mathbb{R}^3$,

Table 1: Physical parameters used for the simulations. The parameters can be found in: FFP scanner setup [27] and particle parameters [6].

Parameter		**Value**		
Magnetic permeability	μ_0	$4\pi \times 10^{-7}$ H/m		
Boltzmann constant	k_B	$1.38064852 \times 10^{-23}$ J/K		
Particle				
Temperature	T_B	293 K		
Sat. magnetization	M_S	474000 J/m^3/T		
Particle core diameter	D	$\in \{20, 30, 40\} \times 10^{-9}$ m		
Particle core volume	V_C	$1/6\pi D^3$		
	m_0	$\frac{1}{\mu_0}$		
	β	$\frac{\mu_0 V_\mathrm{C} M_\mathrm{S}}{k_\mathrm{B} T_\mathrm{B}}$		
Geometry	d	1	2	3
FOV	e_1	$[-12.5, 12.5]$ mm	$[-12.5, 12.5]$ mm	$[-12.5, 12.5]$ mm
	e_2	–	$[-12.5, 12.5]$ mm	$[-12.5, 12.5]$ mm
	e_3	–	–	$[-6.5, 6.5]$ mm
Cuboid size	Δx	0.1 mm	0.5×0.5 mm^2	$1.0 \times 1.0 \times 1.0$ mm^3
Scanner FFP case				
Excitation frequencies	f_1	$2.5/102 \times 10^6$ Hz	$2.5/102 \times 10^6$ Hz	$2.5/102 \times 10^6$ Hz
	f_2	–	$2.5/96 \times 10^6$ Hz	$2.5/96 \times 10^6$ Hz
	f_3	–	–	$2.5/99 \times 10^6$ Hz
Excitation amplitudes	A_1	0.012 T/μ_0	0.012 T/μ_0	0.012 T/μ_0
	A_2	–	0.012 T/μ_0	0.012 T/μ_0
	A_3	–	–	0.012 T/μ_0
Gradient strength	$G_{1,1}$	-1 T/m/μ_0	-1 T/m/μ_0	-1 T/m/μ_0
	$G_{2,2}$	-1 T/m/μ_0	-1 T/m/μ_0	-1 T/m/μ_0
	$G_{3,3}$	2 T/m/μ_0	2 T/m/μ_0	2 T/m/μ_0
Measurement time	T	0.04×10^{-3} s	0.653×10^{-3} s	21.54×10^{-3} s
	Δt	0.01×10^{-6} s	0.2×10^{-6} s	0.4×10^{-6} s
Scanner FFL case				
Excitation frequencies	f_1	–	–	–
	f_2	–	$2.5/96 \times 10^6$ Hz	$2.5/96 \times 10^6$ Hz
	f_3	–	–	$2.5/96/25/20 \times 10^6$ Hz
Field rotation	f_rot	–	2604.17 Hz	2604.17 Hz
Excitation amplitudes	A_1	–	–	–
	A_2	–	0.012 T/μ_0	0.012 T/μ_0
	A_3	–	–	0.06 T/μ_0
Gradient strength	$G_{1,1}$	–	0 T/m/μ_0	0 T/m/μ_0
	$G_{2,2}$	–	-1 T/m/μ_0	-1 T/m/μ_0
	$G_{3,3}$	–	1 T/m/μ_0	1 T/m/μ_0
Measurement time	T	–	0.77×10^{-3} s	19.2×10^{-3} s
	Δt	–	0.2×10^{-6} s	0.4×10^{-6} s

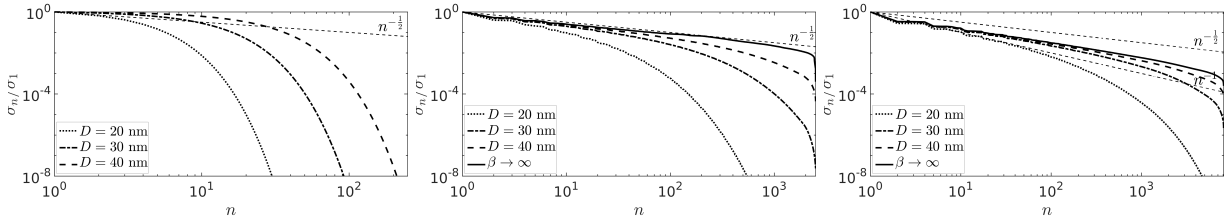

(a) FFP 1D (b) FFP 2D (c) FFP 3D

Figure 3: SV decay for triangular excitation patterns and different particle diameters in (a) 1D, (b) 2D, and (c) 3D domains.

i.e., $g(x,t) = P(t)^t G P(t) x$, with $P : I \to \mathbb{R}^{3\times 3}$ given by

$$P(t) = \begin{pmatrix} \cos(2\pi f_\mathrm{rot} t) & \sin(2\pi f_\mathrm{rot} t) & 0 \\ -\sin(2\pi f_\mathrm{rot} t) & \cos(2\pi f_\mathrm{rot} t) & 0 \\ 0 & 0 & 1 \end{pmatrix}$$

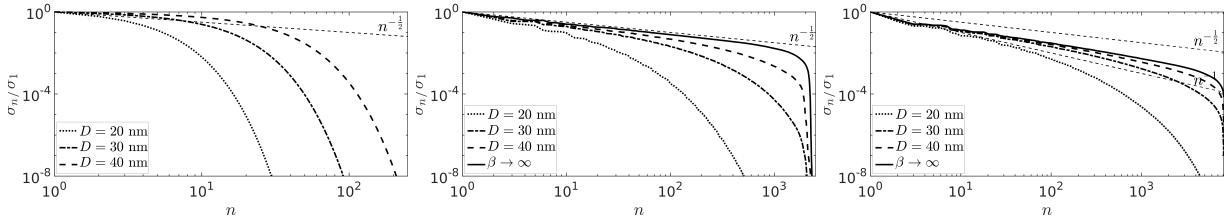

(a) FFP 1D (b) FFP 2D (c) FFP 3D

Figure 4: SV decay for sinusoidal excitation patterns and different particle diameters D, with one single receive coil in (a) 1D, (b) 2D, and (c) 3D domains.

for $f_{\text{rot}} > 0$. A translational movement is performed by using a drive field perpendicular to the FFL at any time $t \in I$. Assuming $G_{1,1} = 0$, the non-rotated FFL is the e_1-axis and we obtain the rotated drive field

$$h(t) = -P(t)^t \tilde{h}(t) = -A_2 \sin(2\pi f_2 t)(-\sin(2\pi f_{\text{rot}} t), \cos(2\pi f_{\text{rot}} t), 0)^t - A_3 \sin(2\pi f_3 t) e_3.$$

for a non-rotated drive field $\tilde{h}(t) = (0, A_2 \sin(2\pi f_2 t), A_3 \sin(2\pi f_3 t),\ A_2, A_3, f_2, f_3 > 0$. The parameters used to obtain the FFL results are given in Table 1. We use measurement times comparable to the FFP case. The rotation frequency f_{rot} is chosen such that two complete rotations are performed during the whole measurement time in 2D. In 3D, a slowly varying field moves the FFL plane in e_3-direction. The corresponding frequency f_3 is chosen such that the field's period is the whole measurement time. Since the rotation matrix $P(t)$ depends smoothly on time t, it does not influence the analysis in Theorem 4.4. The numerical results are given in Fig. 5. It is observed that the SVs decay slower, when the particle diameter D increases. In 2D we observe a decay rate slightly slower than $O(n^{-\frac{1}{2}})$ for the leading SVs for the largest diameter. Qualitatively, the 3D limit case agrees with the prediction in Theorem 4.4 but it does not completely approach $O(n^{-\frac{1}{4}})$ (the sharp one is conjectured to be $O(n^{-\frac{1}{2}})$; see Remark 4.2).

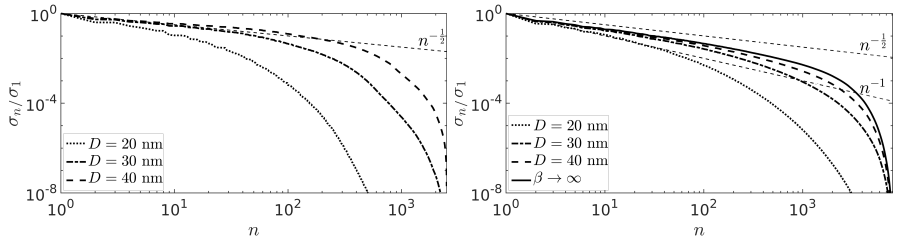

(a) FFL 2D (b) FFL 3D

Figure 5: SV decay for sinusoidal FFL excitation patterns and different particle diameters in (a) 2D and (b) 3D domains.

Last, we compare the FFP and FFL cases. The comparative results in Fig. 6 show clearly the slower SV decays for the leading SVs for the FFL case for one example particle diameter in 2D and the limit case in 3D. Equivalently, for a given noise level, there are more significant singular values in the FFL case than in the FFP case, which potentially allows obtaining higher resolution reconstructions.

6 Discussions and concluding remarks

In this work, we have analyzed the nonfiltered MPI equilibrium model with common experimental setup, and studied the degree of ill-posedness of the forward operator via SV decay for Sobolev smooth bivariate functions. Our analysis gives rise to the following findings. The standard setup in MPI using trigonometric drive field patterns and a linear selection field leads to a severely ill-posed problem. For the nonfiltered model, even if the trajectories $h(t)$ are nonsmooth, for the linear selection field, Theorem 4.2 predicts a

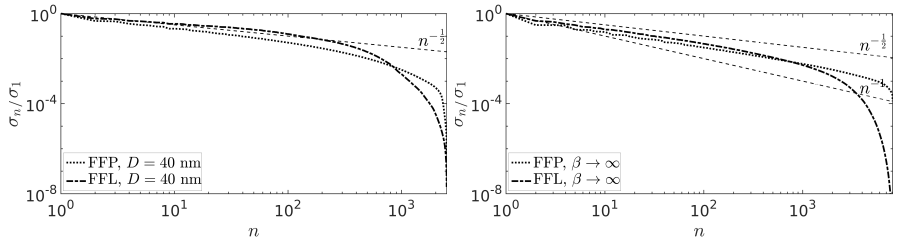

(a) FFP vs. FFL 2D (b) FFP vs. FFL 3D

Figure 6: The comparison of SV decay for the FFP and FFL cases with sinusoidal excitation patterns in (a) 2D and (b) 3D domains.

SV decay faster than any polynomial. The resolution improvement for larger diameters reported in [43, 23] can be explained by considering the limit case. Two different MPI methodologies, i.e., FFP and FFL, are distinguished in this work, where the FFL case has not been studied theoretically before. The FFL approach can potentially lead to a less ill-posed problem than the FFP approach (Theorems 4.3 and 4.4). In the discrete setup, the temporal behavior of the FFL needs to be chosen more carefully to fully exploit the potential benefits predicted by the limit case. In particular, this has to be considered when parameterizing the FFL case with respect to hardware limitations, e.g., rotation frequency [3]. Further, a theoretical result for the filtered problem exhibits a faster SV decay for analog filters with high (temporal) regularity.

The theoretical findings in this work build the basis for several directions of further research of both theoretical and empirical nature. First, the predicted severe ill-posedness for small particle diameters opens the avenue for developing more efficient algorithms based on low-rank approximations of the forward operator. Second, the techniques are fairly general and might also be employed to analyze other more refined models for MPI, which include particle dynamics and particle-particle interactions [21]. Last, for image reconstruction, it is natural to analyze regularized formulations in the context of regularization theory [8, 19].

Acknowledgements

The authors are grateful to the referee and the board member for constructive comments, which have improved the quality of the work. T. Kluth is supported by the Deutsche Forschungsgemeinschaft (DFG) within the framework of GRK 2224/1 "Pi^3 : Parameter Identification - Analysis, Algorithms, Applications", and G. Li partially by Hausdorff Center for Mathematics, University of Bonn and a Newton international fellowship from Royal Society.

References

[1] M. Abramowitz and I. A. Stegun. *Handbook of Mathematical Functions with Formulas, Graphs, and Mathematical Tables*. Dover, New York, 1964.

[2] R. A. Adams and J. J. F. Fournier. *Sobolev Spaces*. Elsevier/Academic Press, Amsterdam, second edition, 2003.

[3] A. Bakenecker, T. Friedrich, M. Graeser, J. Stelzner, and T. M. Buzug. Experimental validation of the selection field of a rabbit-sized FFL scanner. *Int. J. Magn. Part. Imag.*, 3(1):1703013, 5 pp., 2017.

[4] A. Behzadan and M. Holst. Multiplication in Sobolev spaces, revisited. Preprint, arXiv:1512.07379v2, 2017.

[5] V. I. Burenkov. Estimates for Fourier transforms and convolutions in Nikol′skiĭ-Besov spaces. *Trudy Mat. Inst. Steklov.*, 187:31–38, 1989.

[6] R. J. Deissler, Y. Wu, and M. A. Martens. Dependence of Brownian and Néel relaxation times on magnetic field strength. *Med. Phys.*, 41(1):012301, 13 pp, 2014.

[7] V. Dicken and P. Maass. Wavelet-Galerkin methods for ill-posed problems. *J. Inv. Ill-Posed Problems*, 4(3):203–221, 1996.

[8] H. W. Engl, M. Hanke, and A. Neubauer. *Regularization of Inverse Problems*. Kluwer, Dordrecht, 1996.

[9] W. Erb, A. Weinmann, M. Ahlborg, C. Brandt, G. Bringout, T. M. Buzug, J. Frikel, C. Kaethner, T. Knopp, T. März, M. M, M. Storath, and A. Weber. Mathematical analysis of the 1D model and reconstruction schemes for magnetic particle imaging. *Inverse Problems*, 34(5):055012, 21 pp., 2018.

[10] G. B. Folland. *Real Analysis: Modern Techniques and their Applications*. John Wiley & Sons, New York, 1999.

[11] B. Gleich and J. Weizenecker. Tomographic imaging using the nonlinear response of magnetic particles. *Nature*, 435(7046):1214–1217, 2005.

[12] I. C. Gohberg and M. G. Kreĭn. *Introduction to the Theory of Linear Nonselfadjoint Operators*. AMS, Providence, R.I., 1969.

[13] M. Griebel and H. Harbrecht. Approximation of bi-variate functions: singular value decomposition versus sparse grids. *IMA J. Numer. Anal.*, 34(1):28–54, 2014.

[14] M. Griebel and G. Li. On the decay rate of the singular values of bivariate functions. *SIAM J. Numer. Anal.*, 56(2):974–993, 2018.

[15] J. Haegele, J. Rahmer, B. Gleich, J. Borgert, H. Wojtczyk, N. Panagiotopoulos, T. Buzug, J. Barkhausen, and F. Vogt. Magnetic particle imaging: visualization of instruments for cardiovascular intervention. *Radiology*, 265(3):933–938, 2012.

[16] B. Hofmann and S. Kindermann. On the degree of ill-posedness for linear problems with non-compact operators. *Methods Appl. Anal.*, 17(4):445–461, 2010.

[17] B. Hofmann and O. Scherzer. Factors influencing the ill-posedness of nonlinear problems. *Inverse Problems*, 10(6):1277–1297, 1994.

[18] T. Hytönen, J. van Neerven, M. Veraar, and L. Weis. *Analysis in Banach Spaces*. Springer, 2016.

[19] K. Ito and B. Jin. *Inverse Problems: Tikhonov Theory and Algorithms*. World Scientific, Hackensack, NJ, 2015.

[20] A. Khandhar, P. Keselman, S. Kemp, R. Ferguson, P. Goodwill, S. Conolly, and K. Krishnan. Evaluation of PEG-coated iron oxide nanoparticles as blood pool tracers for preclinical magnetic particle imaging. *Nanoscale*, 9(3):1299–1306, 2017.

[21] T. Kluth. Mathematical models for magnetic particle imaging. *Inverse Problems*, 34(8):083001, 27 pp., 2018.

[22] T. Kluth and P. Maass. Model uncertainty in magnetic particle imaging: Nonlinear problem formulation and model-based sparse reconstruction. *Int. J. Magnetic Particle Imag.*, 3(2):707004, 10 pp., 2017.

[23] T. Knopp, S. Biederer, T. Sattel, and T. M. Buzug. Singular value analysis for magnetic particle imaging. In *Nuclear Science Symp. Conf. Record, 2008. NSS'08. IEEE*, pages 4525–4529, 2008.

[24] T. Knopp and T. M. Buzug. *Magnetic Particle Imaging: An Introduction to Imaging Principles and Scanner Instrumentation*. Springer, Berlin/Heidelberg, 2012.

[25] T. Knopp, M. Erbe, T. F. Sattel, S. Biederer, and T. M. Buzug. A Fourier slice theorem for magnetic particle imaging using a field-free line. *Inverse Problems*, 27(9):095004, 14 pp., 2011.

[26] T. Knopp, N. Gdaniec, and M. Möddel. Magnetic particle imaging: from proof of principle to preclinical applications. *Phys. Med. Biol.*, 62(14):R124–R178, 2017.

[27] T. Knopp, T. Viereck, G. Bringout, M. Ahlborg, J. Rahmer, and M. Hofmann. MDF: Magnetic particle imaging data format. Preprint, arXiv:1602.06072, 2016.

[28] H. König. *Eigenvalue Distribution of Compact Operators*. Birkhäuser Verlag, Basel, 1986.

[29] M. A. Krasnosel'skiĭ, P. P. Zabreĭko, E. I. Pustyl'nik, and P. E. Sobolevskiĭ. *Integral Operators in Spaces of Summable Functions*. Noordhoff International Publishing, Leiden, 1976.

[30] A. K. Louis. *Inverse und schlecht gestellte Probleme*. B. G. Teubner, Stuttgart, 1989.

[31] N. Löwa, P. Radon, O. Kosch, and F. Wiekhorst. Concentration dependent MPI tracer performance. *Int. J. Magnetic Particle Imag.*, 2(1):601001, 5 pp., 2016.

[32] T. März and A. Weinmann. Model-based reconstruction for magnetic particle imaging in 2D and 3D. *Inv. Probl. Imag.*, 10(4):1087–1110, 2016.

[33] P. Mathé and B. Hofmann. Direct and inverse results in variable Hilbert scales. *J. Approx. Theory*, 154(2):77–89, 2008.

[34] W. J. Morokoff and R. E. Caflisch. Quasi-Monte Carlo integration. *J. Comput. Phys.*, 122(2):218–230, 1995.

[35] K. Murase, M. Aoki, N. Banura, K. Nishimoto, A. Mimura, T. Kuboyabu, and I. Yabata. Usefulness of magnetic particle imaging for predicting the therapeutic effect of magnetic hyperthermia. *Open J. Med. Imag.*, 5(2):85, 2015.

[36] A. B. Owen. Quasi-Monte Carlo for integrands with point singularities at unknown locations. In *Monte Carlo and Quasi-Monte Carlo Methods 2004*, pages 403–417. Springer, Berlin, 2006.

[37] A. Pietsch. *Eigenvalues and s-Numbers*. Cambridge University Press, London, 1987.

[38] J. Salamon, M. Hofmann, C. Jung, M. G. Kaul, F. Werner, K. Them, R. Reimer, P. Nielsen, A. vom Scheidt, G. Adam, T. Knopp, and H. Ittrich. Magnetic particle/magnetic resonance imaging: in-vitro MPI-guided real time catheter tracking and 4D angioplasty using a road map and blood pool tracer approach. *PLOS one*, 11(6):e0156899–14, 2016.

[39] E. M. Stein and G. Weiss. *Introduction to Fourier Analysis on Euclidean Spaces*. Princeton University Press, Princeton, N.J., 1971.

[40] K. Them, M. G. Kaul, C. Jung, M. Hofmann, T. Mummert, F. Werner, and T. Knopp. Sensitivity enhancement in magnetic particle imaging by background subtraction. *IEEE Trans. Med. Imag.*, 35(3):893–900, 2016.

[41] H. Triebel. *Interpolation Theory, Function Spaces, Differential Operators*. North-Holland, Amsterdam-New York, 1978.

[42] G. Wahba. Ill-posed problems: numerical and statistical methods for mildly, moderately and severely ill-posed problems with noisy data. Tech. Rep. No. 595, Department of Statistics, University of Wisconsin Madison, `http://www.stat.wisc.edu/~wahba/ftp1/oldie/595.pdf`, 1980.

[43] J. Weizenecker, J. Borgert, and B. Gleich. A simulation study on the resolution and sensitivity of magnetic particle imaging. *Phys. Med. Biol.*, 52(21):6363–6374, 2007.

[44] J. Weizenecker, B. Gleich, and J. Borgert. Magnetic particle imaging using a field free line. *J. Phys. D: Appl. Phys.*, 41(10):105009, 3 pp., 2008.

[45] J. Weizenecker, B. Gleich, J. Rahmer, H. Dahnke, and J. Borgert. Three-dimensional real-time in vivo magnetic particle imaging. *Phys. Med. Biol.*, 54(5):L1–L10, 2009.

[46] K. Yosida. *Functional Analysis*. Springer-Verlag, Berlin-New York, 1980.

[47] E. Y. Yu, M. Bishop, B. Zheng, R. M. Ferguson, A. P. Khandhar, S. J. Kemp, K. M. Krishnan, P. W. Goodwill, and S. M. Conolly. Magnetic particle imaging: a novel in vivo imaging platform for cancer detection. *Nano Letters*, 17(3):1648–1654, 2017.

[48] Z. Zhang. How many numerical eigenvalues can we trust? *J. Sci. Comput.*, 65(2):455–466, 2015.